Tech Memo
Mat/Str 1163

Tech Memo
Mat/Str 1163

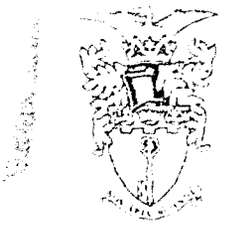

14

ROYAL AEROSPACE ESTABLISHMENT

Technical Memorandum

February 1991

Evolution of a Voltage-Time Model of Thermal Batteries

by

J. Knight

Procurement Executive, Ministry of Defence
Farnborough, Hampshire

ROYAL AEROSPACE ESTABLISHMENT

Technical Memorandum Mat/Str 1163

Received for printing 14 February 1991

EVOLUTION OF A VOLTAGE-TIME MODEL OF THERMAL BATTERIES

by

J. Knight

SUMMARY

A temperature-time model of thermal batteries has almost been completed and validated against experimental data. This Memorandum first summarises early attempts to integrate a voltage-time model into this, taking advantage of the instantaneous predictions of temperature, thermodynamic potentials, and internal resistance which the thermal model provides. It then describes how recent refinements of the voltage-time model have led to improved simulation of the discharges of a wide range of sizes and types of thermal battery under an equally wide range of test conditions.

The semi-empirical approach adopted has been to provide a universally-applicable framework based on logical concepts to cover various effects such as polarisation etc, but with adjustable numerical parameters. It is shown that a moderately good simulation may be obtained for the majority of available discharge curves, using this one set of equations and without altering parameter values. Further improvements can be obtained when parameter values are optimised for one particular type of battery.

Comparisons of model simulations against a body of experimental data have pinpointed remaining discrepancies which will guide further refinement efforts.

LIST OF CONTENTS

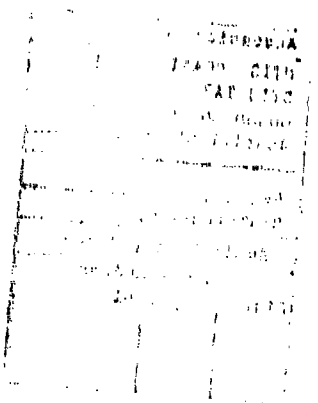

CONDITIONS OF RELEASE

0096948 300873

MR PAUL A ROBEY
DTIC
Attn:DTIC-FDAC
Cameron Station-Bldg 5
Alexandria
VA 22304 6145
USA

********** DRIC U

********** DRIC Y

Reports quoted are not necessarily available to members of the public or to commercial organisations.

1 INTRODUCTION

Thermal batteries were developed after World War II as the preferred power source for various functions on guided missiles. They are active at temperatures of typically 500°C and rely on molten salt eutectics such as lithium chloride-potassium chloride in order to supply significant power[1]. Thus, compared with most other types of battery, their performance is more than usually influenced by temperature. This might severely curtail their active lives if the salt eutectic solidifies on cooling before their electroactive materials are exhausted. Equally, too high a peak temperature during battery activation may result in premature battery failure. Another factor which is more extreme in thermal battery discharges than in other types is the wide range of temperature experienced by their cells throughout their active life. This varies according to application, ambient temperature, and size of battery, but might typically be from 550 down to 400°C or below. Lastly, the heat which eventually warms up the battery outer container may sometimes pose a problem for the immediate surroundings of the battery.

From the above considerations, it is seen that a temperature-time model of thermal batteries can of itself be a considerable aid to the thermal battery designer. Predicting the temperature of older battery designs using the calcium/calcium chromate electrochemical couple was difficult because of the extensive chemical side reactions which occur. However, their increasing replacement by lithium/iron disulphide designs reduced these, simplifying the prediction of battery temperature and performance. Several organisations have published their efforts on thermal modelling of thermal batteries, including Sandia Laboratories[2]. Their model which predicted temperature distributions during the cooling phase was extended when RAE simulated the large temperature gradients built up during activation by a pyrotechnic charge[3]. Predictions were then available of the differing heating rates of the various cell components, their peak temperatures, and of the overall activation time for different designs. More recently[4] RAE effort has focussed on validating the thermal model during the subsequent cooling phase against experimental thermocouple data generated from both electrically-inactive and -active batteries. Quite good simulations of battery temperature are now available using this for a wide range of battery designs and electrical load profiles. This is now regarded as almost complete, the major deficiency being that further study would be desirable of the extent of chemical side-reactions such as cathode pyrolysis within the thermal battery environment, as opposed to

open systems with inert-gas flow, such as the pan of a thermogravimetric analyser[5]. Further discussion of exothermic side-reactions, as they affect the voltage-time model, is given in sections 6.1 and 7.2.

The final aim of thermal battery modelling studies at RAE continues to be the provision of an integrated temperature and voltage model which is capable of reasonably accurate prediction for a wide range of batteries and test conditions. This Memorandum describes a further stage in the improvement of the voltage-time model, as well as documenting how this stage has evolved, and the approach adopted. The advantage of the model when finalised should be that the process of optimising new designs for new applications should be speeded up, with an attendant cost saving; it should also aid research on new configurations and should increase the confidence with which designs outside the presently-known range might be configured. All this can be assessed 'on paper' before prototypes are manufactured and tested.

2 DESIGN AND PERFORMANCE DATA BANK

In essence, the RAE model is fed detailed information on the battery design, and on the chosen electrical load profile and other test conditions; it then predicts battery performance. A body of combined design and performance data is thus essential against which to test the effect of model changes. As the aim is to eventually model a wide range of battery types and test conditions, this data bank should also cover the full range. RAE do not manufacture thermal batteries, not even experimental prototypes, so the experimental data quoted in this Memorandum is necessarily limited and has either been reproduced by permission from thermal battery manufacturers' own tests, or has been obtained by RAE discharge tests on their products.

Nevertheless, the 11 battery designs studied span a range of outside diameters from 18 to 91 mm, employ lithium-iron, lithium-aluminium or lithium-silicon as anode materials, but all use iron disulphide as the cathode. Likewise, the 16 discharge test conditions range from ambient temperatures of -45 to +74^{o}C, and electrical load profiles ranging from continuous constant-current or constant-resistive loads to periodic sequences of short pulses. The designs are not necessarily regular production designs, nor are the load profiles necessarily representative of any particular application. Table 1 gives some information on these battery tests, and indicates whether temperature or capacity exhaustion were predicted to be the life-limiting factor under the conditions employed.

3 THEORETICAL CONTENT OF THE VOLTAGE-TIME MODEL

Ideally, computer models should be developed entirely according to established theories, so that they might eventually have good predictive power beyond the presently-known limits, and might considerably increase understanding of how observed discharges are derived. It was a practical proposition to base the thermal model almost entirely on the well-known theories of heat transfer, thermodynamics of electrochemical cells etc, so that an *ab initio* model could be developed in a reasonable time.

This would also be the ideal for the voltage-time model. Lawrence Berkeley Laboratory, California have described one such model of flooded-electrolyte lithium alloy-iron disulphide cells operated isothermally[6]. This is developed from their earlier model of iron monosulphide cells[7], and considers details of the volume make-up and porosity of the electrodes, diffusion rates within them, and the effects of phase precipitation on performance. The impetus for their work was the optimisation of the large secondary well-insulated batteries intended for vehicle propulsion, rather than the comparatively short-lived smaller primary thermal batteries which would usually experience a more variable temperature during their active lives.

At the other extreme, Shepherd[8] and others have shown how good fits to observed discharges of several types of battery may be obtained by purely empirical equations with fitting parameters readjusted for each type, and without any reference to the thermodynamics of the cell reaction. In deciding which approach might be most practical to adopt for thermal batteries, the following features of thermal battery discharges (some of which are experimental observations and some likely hypotheses) might usefully be listed:

(i) the discharge of iron disulphide cathode can be highly inhomogeneous[9];

(ii) experimental discharge curves can be significantly modified by additives[9], or even by different particle sizes or batches of active material;

(iii) the possibility exists of hidden leakage currents (shorting) during the active life of thermal batteries;

(iv) the electrodes and separator are porous multi-phase bodies, and discharge, which depends on migration of species through them, could well be influenced by factors like aspect ratio, void content[6], wettability etc.

Although this list is not meant to be exhaustive, it gives sufficient indication that an attempt to provide a truly theoretical model of thermal battery discharges might not be cost-effective, since at least some of the above effects could be ill-defined and/or difficult to determine.

It was therefore considered best to provide a theoretical framework for the gross effects such as Faraday's Law, cell thermodynamics, and internal resistance which are relatively simple to treat theoretically, whilst complementing this with a semi-empirical treatment of effects such as polarisation. Where possible this semi-empirical portion is based on physically reasonable ideas and the aim has been to set up equations having general applicability for all conditions met. These equations contain numerical parameters which are set by fitting procedures. Ideally, the same numerical values would then be valid over all conditions, but otherwise there should at least be some category of conditions (for example batteries from one particular manufacturer, or one particular combination of pellet material compositions) over which reliable predictions could be made. The extent to which these aims have been achieved in the latest model version is apparent in section 6.

4 PRELIMINARY VOLTAGE-TIME MODELS

The thermal and electrical behaviour of thermal batteries are interdependent in a number of important respects:

(i) the passage of current through the battery generates heat;

(ii) the equilibrium potentials of both electrodes are temperature-dependent;

(iii) the active lifetime of the battery may be linked to the freezing of molten salts;

(iv) the internal resistance of the battery depends on temperature.

The aim of the first voltage model was simply to estimate the rate of heat generation caused by current flow, as in (i) above, and so to improve the thermal model. The magnitude and effect of this can be very considerable for large batteries discharged at high rates, even to the extent of causing a net temperature rise within the cells as the discharge proceeds, as this heating effect can more than offset the natural cooling of the battery according to Newton's Law. In this version the internal resistance value was a constant supplied by the user.

In the first major attempt to develop a voltage-time model *per se*, discharge curves from isothermal single-cell tests were analysed and a number of

concepts affecting the cell capacity and voltage were inferred and expressed in mathematical form. These included the variation of internal resistance with both temperature and state-of-discharge, and the degradation/under-utilisation of theoretical capacity as a function of current density above a certain threshold. Thermodynamic potentials were calculated only for the complete cell, not for individual electrodes, so it was assumed that there was always an exact balance of theoretical capacity between the two. Whilst good simulations were initially obtained over a narrow range of battery types, it was soon clear that this model would not find more general applicability, and was therefore discontinued.

5 MARK II VOLTAGE-TIME MODEL

The main improvement here over the previous attempts was to base the calculation on a sounder theoretical footing by treating each electrode individually and incorporating literature equations[9,10], defining the various electrode potentials as a function of both state-of-discharge and temperature. This automatically catered for battery designs in which the electrodes were unbalanced in theoretical capacity. Apart from this, this version essentially computed the discharge curve one might expect from a battery in which the active ingredients were 100% utilised, without any kinetic limitation, and assuming no dissipation of theoretical capacity other than usefully through the external load. As a minor variant incorporated later, an ability to simulate short-circuit paths was provided, if a constant resistance value was entered. The Mark II model was therefore too optimistic for manufactured batteries, as expected, except in the important case where the test conditions imposed cell cooling as the factor limiting the battery life. This case was already simulated by the existing thermal model and examples of its effects have already been given[4] and are also shown later. Whilst being too optimistic for discharges which are not limited by temperature, this version was of interest in comparing experimental discharges with the theoretical limit, in order to assess energy efficiency more clearly.

The following steps summarise how the prediction of on-load voltage is derived:

(i) the user defines the dimensions and densities of cell component pellets in his input data;

(ii) the user also specifies a number of either constant-current or constant-resistive loads (or a combination of both) together with the time periods during which each operates;

(iii) from (i) the theoretical capacities of both electrodes are computed (for pellets with the minimum specified dimensions).

(iv) the number of cells is derived by counting the number of electrolyte/cathode interfaces in the user's design grid;

(v) adjustments are made to all affected variables (number of cells, current, internal resistance) according to whether the user chose a quarter- or half-section grid, or whether he specified one series string of cells, or two equal stacks connected in parallel;

(vi) the iterative process which recalculates each variable at increasing times begins;

(vii) the current flowing through the cells is computed, in cases (*eg* short-circuiting), where it is not identical to that in the external circuit, and for either type of external load;

(viii) from (vii), a running tally is kept of discharged capacity, and resistive heating and entropic cooling are estimated;

(ix) temperature distributions are calculated, corrected for phase changes, and a single-value 'cell temperature' is defined as the mean of the maximum and minimum cathode temperatures;

(x) a state-of-discharge is defined as the ratio of the discharged capacity to that theoretically available from a 1-electron transfer in the computed amount of active material in each electrode[9];

(xi) a thermodynamic equilibrium potential for each electrode is computed from the literature equations mentioned above[9,10];

(xii) the cell and battery emfs are defined from the algebraic sum of electrode potentials;

(xiii) numerical values are assigned to the bulk resistivities of all cell component pellets. These are a mixture of inferred values from a report[9] together with arbitrary interim values pending better measurements. The values used, in ohm cm, were:

Pellet material	Resistivity	Reference
lithium/iron	0.3	
lithium/aluminium or lithium/silicon	0.5	
iron disulphide cathode pellets	1.4	9
all electrolyte pellets	2.68	9
burnt pyrotechnic pellets	1.0	
metallic cups or discs	0.1	

(The variation of cathode resistance with state-of-discharge quoted in a report[9] was also incorporated, but was withdrawn after it resulted in poorer results for

one or two batteries simulated. A possible reason for this has now been given, as discussed in section 6.4.)

(xiv) the above electrolyte resistivity is then modified if, after inspection of the temperature of every electrolyte grid element, it is found that salt eutectic would either be within or below the freezing range in the element. These extra contributions are then summed across each cell pellet, and then down each series string of cells, in order to estimate the total effect of salt freezing, if any, throughout the battery;

(xv) an interim internal resistance for the whole battery (irrespective of type of design grid or electrical connection) is then computed from the resistivity data ((xiii), (xiv)) and from the pellet dimensions the user specified (i). This is then corrected for temperature;

(xvi) an on-load voltage is then estimated at each sample time from the simple formula

$$V = V' - IR \quad , \qquad (1)$$

where V is the battery on-load voltage,
V' is the battery thermodynamic equilibrium potential (xii),
I is the current flowing through the cells (vii)
and R is the corrected internal resistance (xv) at the cell temperature (ix);

(xvii) to balance economy of computing time with the ability to calculate and display pulse shapes, a programme of calculation times is set up, in which the interval between successive calculations starts increasing by 2% each time once the large temperature gradients formed during activation have subsided. At the approach to each electrical load change specified by the user, this programme is temporarily interrupted so that a calculation may be done immediately on either side of the load change. Afterwards the programme of expanding calculation intervals is made to resume from the value it reached just before the load change occurred;

(xviii) the on-load voltage (as well as temperature distributions and other heat loss parameters) are sampled at all times specified by the user, and automatically on either side of each electrical load change, whether they were specifically requested or not.

The effects of applying the Mark II model to the discharges of seven different battery designs (Table 1, Batteries 1-7) discharged on either continuous or pulsed loads are shown in Figs 1 to 3. (Except where otherwise stated, all solid traces in the Figures represent experimental data; broken traces are model simulations.) The following features of the simulations may be listed:

(i) too low a battery voltage is predicted immediately after activation for some batteries (Fig 2, battery 2; Fig 3). This is probably due to the well-known 'voltage spike' effect which the model does not allow for;

(ii) after this has gone, the model estimates the battery voltage quite well early in discharge life (Figs 2 and 3), and where it is possible to check on the magnitude of internal resistance (Fig 2, battery 2; Fig 3) the resistivity values quoted above provide quite a close estimate. This is especially apparent for battery 3 in Fig 3. Thus the calculations of both thermodynamic potentials and internal resistance are reasonably accurate early in life;

(iii) there is a consistent tendency for the simulated battery voltage to remain steady in later life, whereas in reality it gradually falls away sooner than was predicted. The only exception seen is one of the predicted discharges of battery 6 in Fig 2 (which differ only in test temperature), which was predicted to be temperature-limited due to the low ambient temperature;

(iv) for batteries subjected to regular but occasional pulses on top of an otherwise low or zero background current (Fig 3), and which are predicted to be temperature-limited, the Mark II model provides for an increased internal resistance as eventually observed, but in the simulation this appears too early in life and increases too suddenly in magnitude.

Similar trends were observed for the other few batteries in Table 1. Fig 1 shows how this model naturally leads to the formation of 'square' pulses rather than the ones observed experimentally. It is also seen that in most cases, too optimistic a duration would have been predicted to any particular voltage cut-off. The next section describes how some at least of these inadequacies were addressed.

6 MARK III VOLTAGE-TIME MODEL

This enhancement over the Mark II version provides a preliminary treatment of polarisation, reintroduces a simpler concept of capacity degradation, makes allowance for manufacturing tolerances, and revises the presentation of results.

6.1 Capacity degradation

Comparison between the theoretical capacity of batteries, their observed duration to exhaustion, and the amount of residual lithium metal estimated from post-mortem analysis after the battery has cooled shows that the active materials can be partially consumed at the same time as they provide useful electrical output[11]. There is also evidence from a very limited number of tests that the degradation rate can be approximately constant.

Allowance has therefore been made in the model for the theoretical state-of-discharge to be enhanced by this amount, whose magnitude is governed by an adjustable parameter specifying the percentage of anode capacity degraded per minute of discharge duration. The state-of-discharge of both electrodes is simultaneously increased, so it is assumed that whatever the mechanism for the capacity loss, it involves lithium and iron disulphide in the same relative proportions as the nominal electrical discharge reaction on the upper voltage plateau. All simulations shown in Figs 4 to 14 (except Fig 11) are based on the same fixed capacity degradation rate of a fraction of a per cent of lithium theoretical capacity per min. Experimental evidence[11] showed that this was the appropriate rate for one particular battery, and it is encouraging that this figure is broadly in agreement with the range recently quoted[12] for isothermal single-cells stood on open-circuit before discharge. This range of between 2.5 and 10 coulombs/min between 450 and 550°C for small cells containing different salt eutectics equates to 0.06 to 0.23 or 0.2 to 0.8% of lithium capacity per min, depending on whether the whole of the lithium in the anode, or only that fraction of it associated with the relevant constant-potential phase transition, is considered.

No thermal effects of this capacity loss were taken into account in the simulations shown in these Figures; this possibility is, however, considered in section 7.2.

6.2 Allowance for time-dependent polarisation

The impetus for this refinement arose from RAE tests on Battery 1, since it was seen in section 5 that the Mark II model simulated this battery poorly (Fig 1). In this test, the following conditions were arranged to be met:

(i) the battery was fully discharged before cooling ended its life;

(ii) the current density was set so that the resistive heating rate in the cells balanced the natural cooling rate according to Newton's law, as predicted by the thermal model. The test thus approximated to an isothermal battery discharge, and this was confirmed by a thermocouple placed within the insulating wraps of the battery near

to the perimeter of the cell stack. One variable affecting performance was thereby minimised;

(iii) the current was interrupted as shown in Fig 1 so that pulse shapes could be analysed.

The observed pulses have the following features in common:

(i) when the heavier current is applied over each 50 s in every 60 s cycle, and then switched back to the lighter load for a further 10 s, the voltage soon recovers to a level only slightly below that before starting the pulse sequence, especially after allowance is made for the increase in state-of-discharge during the pulse cycle.

(ii) the relative contributions of the instantaneous versus the time-dependent voltage changes are different for the recovery part of each 60 s cycle from those for the initial voltage dip. Thus, the instantaneous recovery is larger than the instantaneous voltage drop, whilst the range of the time-dependent recovery is smaller than the time-dependent drop;

(iii) the internal resistance/polarisation scarcely increases until the battery is deeply discharged, when the on-load voltage passes through a 'knee' before collapsing;

(iv) the shape of both the polarisation and recovery time-dependent pulse curves may be approximated by exponential decay expressions;

(v) tests on the same battery discharged under other conditions indicated that the magnitude of the time-dependent polarisation/recovery was approximately proportional to the applied current, as is the instantaneous IR drop or rise.

The aim of this version of the model has been to search for a mathematical expression having the appropriate form to cater for continuous and pulsed discharges, with continuous discharges being treated mathematically as a succession of pulses in all of which the current values are identical. The expression should incorporate a time-dependent polarisation/recovery effect as well as merely an instantaneous drop or rise. Restrictions on the form of mathematical expression which can be used automatically result from consideration of the following scenarios. Two model simulations are run, whose only difference is that in the first, a single long time period is chosen, throughout which a single current value (or resistor value) operates; in the second simulation, this same time period is subdivided into two or more segments in the model input data, in all of which the

same current or resistor value operates as in simulation 1. Experience dictates that identical results should be obtained in both cases, and that in the second case, the model should not produce voltage discontinuities at the boundaries between successive time periods.

One expression which obeys this restriction approximately, though not exactly, and yet gives an improved simulation over the Mark II model is:

$$V = V' - IR[1 + a(1 - e^{-bt})] - I'Rce^{-dt} \quad , \qquad (2)$$

where t is the time from the beginning of the last load change,
R is the internal resistance at a particular instant,
I is the current operative in the time period in question,
I' is the current operative in the previous time period
and $a,b,c,$ and d are constants to be fitted with numerical values.

To obey the above mathematical restriction it may be shown that $a = c$ and $b = d$. Obviously I' is undefined in the first time period, so in the Mark III model the second exponential term has been omitted for this period. In physical terms the expression provides an instantaneous drop as in the Mark II model at the beginning of the first time period, and the voltage then undergoes a time-dependent exponential decay at a rate determined by the value of b, to an eventual limit of

$$V = V' - IR \ (t = 0) \rightarrow V = V' - IR(1 + a) \quad (\text{as } t \text{ tends to infinity}).$$

It also resumes with this value at the start of the second time period if the current is unchanged and provided $a = c$ and $b = d$. Provided the first time period is not so short that the voltage is still far from its eventual limit by the end of it, the voltage will have reached approximately this value ensuring no significant discontinuity at the boundary of the first and second time periods.

When the current level in the second time period differs from that in the first, the expression also provides for a recovery curve or further polarisation curve which in broad terms mimicks the actual behaviour of batteries. This is seen in Fig 4, in which curve 1 shows the result of stepping up the current to increasingly higher levels in each successive 60 second period, beginning 5 s after activation. Curve 2 (the solid trace) shows the effect of alternating the fixed current between two different levels in these same time periods, and curve 3 (broken trace) shows that when the simulation of curve 2 is repeated only

using the higher current for all time periods then a smooth prediction without noticeable discontinuities is produced.

With the constants a equal to c and b equal to d , equation (2) unfortunately gives the same voltage span during recovery as during polarisation, which was not the case for Battery 1 as noted above. In concept, equation (2) therefore treats subsequent time periods as a balance between the polarising effect of the present current, opposed by a relaxation or further polarisation from the previous current level, depending on whether it was greater than or less than the present level. This notion, although crude, nevertheless increases the realism of this Mark III version over the Mark II version for nearly all the discharge data available to RAE, as will be shown below.

6.3 Improvements to model procedures, efficiency, and output

The Mark II model (section 5) automatically produced a temperature distribution equal in size to the chosen grid size for each time the results were sampled. The estimated on-load voltage, and eight other single-valued functions specifying heat loss rates and fluxes were also sampled at each time. For designs specified on large grids, and sampled many times, the output is voluminous. A small selection programme is therefore useful to pick out particular features for subsequent plotting.

In order for the Mark III model to reproduce curved pulse shapes it is necessary both to calculate, and to display the results at frequent intervals around the time of each pulse. The previous method (section 5, item (xvii)) of interrupting the expanding time intervals between calculations in order to sample two points either side of a load change would now be inadequate. Instead, the programme has now been modified to operate as follows. It remains as described in section 5 until the first load change specified by the user is approached. If the next calculation time would have exceeded the time of the load change, the interval is reset so as to make the calculation time coincide with this time. The following interval is then reset to an arbitrary 0.5 s. Subsequently, the calculation intervals start expanding again at the same 2% rate each time, but from the reset time of 0.5 s, rather than the point which they had expanded to prior to the onset of the load change. For pulses of less than 1 s in duration, the 0.5 s reset level would need reducing further. Examples of the type of model output produced were shown in Fig 4, and are also seen in subsequent figures.

This modification has two effects: it enables curvature to be reproduced on all but the briefest of pulses, but to do this, the programme needs to perform

more iterations to achieve this greater realism. As the overall computation time increases approximately in proportion to the number of iterations performed (and does not significantly increase due to improvements in the physics during any one iteration), simulations involving large numbers of pulses now take longer to run than previously. Even so, all simulations shown in the Figures were accomplished within a period of 20 to 600 s using the Cray 2 supercomputer at RAE; a typical time would be 100 to 200 s and only the long-duration multi-pulse discharge of battery 3 in Figs 3 and 9 took 600 s. Consideration is now being given to making this Fortran programme available for use on advanced desktop computers[13].

With the Mark III model now calculating and sampling the results at many more times, there was a danger of breaching data storage limits if temperature distributions were also being displayed at all these extra times. Also, whilst there was a need to calculate voltages very frequently around pulses, there was no need to display temperatures so frequently. Hence the Mark III model provides a user-chosen option to either produce output in the form of the Mark II model (with temperatures) or else to merely produce a file of times and voltages suitable for direct plotting, and which can contain thousands of data points.

6.4 Effect of discharge state on internal resistance

In common with other types of battery, thermal batteries tend to exhibit a slight increase in internal resistance with state-of-discharge, as shown in Fig 1. Argonne and Sandia identified the cathode as contributing most to this increase[9], and others[6,14] have shown that the bulk resistivity of its first discharge product, $Li_3Fe_2S_4$, is about 20 times that of iron disulphide. However, as explained for one particular discharge (Fig 31b of Ref 15), the battery internal resistance may only show about a two-fold increase at its peak due to the inhomogeneity of discharge producing different phases simultaneously, and the fact that the subsequent discharge product is much more conductive. Also, if the electrochemical balance between the electrodes is such as to totally deplete the lithium, for example in immobilised liquid-lithium anodes, as the end-of-life approaches, this could be another factor increasing internal resistance.

It was shown, using computer fitting routines, that the experimental pulse shapes from Battery 1 could best be fitted to an expression involving the sum of both exponential and linear terms[16]. This had previously been employed by Shepherd[8]. However, this form of expression does not obey the mathematical restriction noted in section 6.2, since the linear term causes the voltage to drop (or rise), without limit. An alternative, which uses the form of equation (2), is therefore to incorporate the required variation within the internal resistance

function R. Several expressions defining the variation of the temperature-compensated internal resistance with state-of-discharge were therefore evaluated against the body of experimental discharge data. In one case, quite a good fit to the discharge of Battery 1 could be obtained by combining equation (2) with equation (3)

$$R = R'(1 + 1.5Q^2) \quad , \tag{3}$$

where R' is the temperature-corrected internal resistance at the start of discharge, and Q is the state-of-discharge of lithium in the anode ($Q = 0$ at the start of discharge; $Q = 1$ for total lithium exhaustion). This is seen in Fig 5. When equation (3) was subsequently applied to a number of discharges of other batteries (Fig 6), a consistent discrepancy became apparent, though comparison of this Figure with Fig 2 shows a net improvement using the Mark III model over the Mark II version for most discharges. This was that the predicted on-load voltage was too low at low states-of-discharge, but then crossed over the experimental curve in mid-life, and finally became too optimistic near the end of life.

The specific resistivity allocated for the electrolyte pellets (section 5, item (xiii)) was then updated with the figure of ~1.0 Ω cm more recently quoted by Sandia Laboratories[17] for LiCl/KCl/MgO pellets. Simultaneously, other equations for the instantaneous internal resistance were evaluated. One expression which better fitted the discharges of several batteries subjected to continuous loads was

$$R = R'(1 + 2Q + Q^2) \quad . \tag{4}$$

This unfortunately gave a poorer simulation for Battery 1 than that shown in Fig 5, so it appears that this feature may need optimising for each category of battery. As a reasonable compromise, and also to ensure that the battery voltage collapses when the lithium in the anode is exhausted, the form of equation used by Shepherd[8] and others was then adopted

$$R = \frac{R'}{1 - Q} \quad . \tag{5}$$

This automatically provides for a final 'knee' in the discharge curves seen in Battery 1 and some other batteries as the active materials become exhausted, a feature which equations (3) and (4) fail to provide. Figs 7 to 14 show simulations produced by the combination of equations (2) and (5) and with $a = c = 0.7$ and $b = d = 0.2$, for the wide range of battery and test conditions noted above. Comparison of Fig 8 with Figs 2 and 6, and of Fig 7 with Fig 1 shows that the

combination of equations (2) and (5) in the Mark III model affords a further improvement for most of batteries 1 to 6. In no case has this combination significantly worsened the simulation, though comparison of Fig 9 with Fig 3 shows little difference for two batteries subjected to regular short pulses on top of a low background current.

6.5 Effect of manufacturing tolerances

Both electrode active materials can exhibit different discharge plateaux. This is particularly apparent when lithium-silicon/iron disulphide batteries are heavily discharged, as seen in Fig 10. The simulation curves for different external circuit resistors are seen to exhibit sharp 'corners' whereas the corresponding experimental curves are always smoother. In the model, all cells are reaching identical states-of-discharge at the same time, which has generated the discontinuities.

Bernardi and Newman[6] accounted for the rounding of the discharge curves of lithium-silicon/iron disulphide cells in terms of thermodynamic irreversibilities associated with ohmic losses, migration, mass-transfer, and overpotentials. For multi-cell batteries, it is also possible that the greater smoothness of the experimental discharges could be at least partly due to the known scatter in the weights, and hence theoretical capacities, of the active material pellets, due to manufacturing tolerances during the cold-pressing operation.

A new adjustable parameter was therefore provided specifying the range of this tolerance band as a fraction of the mean weight. Then, when the electrode theoretical capacities had been defined in the programme, a population of different capacities within this range was also defined. The definition of battery thermodynamic emf was then based on a calculation of the equilibrium potential of each individual cell in a series string, with its unique theoretical capacity. Initially, a non-random distribution was set up in which the allowable range was equally divided between the required number of cells, with each cell assigned a weight at a different point on this regular distribution. Subsequently, a random number generator routine was called by the programme to provide a completely random distribution in this range.

The effect of this latest modification on the simulation of Battery 8 may be seen by comparing Fig 11 with Fig 10; a closer match has been achieved by incorporation of a very real effect. The simulations in Fig 11 were generated by somewhat reducing the capacity degradation rate from the level used in all other simulations, and also by assigning a maximum spread of pellet weights of 5% either side of the mean. (This was done for illustration only and is not necessarily representative of actual practice.) The simulations shown in Figs 12 to 14

also used this same weight distribution, but reverted to the capacity degradation rate previously used. Fig 12 shows that for Battery 10 in particular, the Mark III model incorporating this effect broadly reproduces the inflexions seen in the experimental discharge curve, as far as it is possible to measure them by ruler from the report (Fig 31a of Ref 15).

7 TEMPERATURE-LIMITED BATTERY DISCHARGES

There is no doubt that the voltage fall-off observed in some discharges may be linked to the freezing of molten salts rather than to active material exhaustion. Table 1 shows which discharges were predicted to be temperature-limited within the timescale of the various figures. In improving the voltage-time model further for such discharges, it is essential to accurately predict the elapsed time before molten salt in the battery re-solidifies. The prediction of this time may be affected by uncertainties in two independent factors - the freezing temperature and the slope of the cooling curve - both of which are discussed below.

7.1 Salt freezing temperature in discharged batteries

There is good agreement, within a few degrees Celsius, about the freezing point of pure salt eutectics such as lithium chloride-potassium chloride. However it is not completely clear at what temperature molten salts freeze in discharged thermal batteries. Experimental evidence using thermocouples has in some cases shown a freezing-point arrest in the cooling curves of cells very close to the theoretical point of 352°C (see for example Fig 12 of Ref 18). A freezing exotherm near to this theoretical temperature was also seen in thermocouple traces for the cooling of electrically-inactive 'dummy' batteries containing LiCl/KCl/MgO and iron/potassium perchlorate pyrotechnic as the only stack components[4]. However, thermocouple measurements from the same study but involving electrically-active batteries suggested that freezing could occur over a range of temperatures below the theoretical point. Contrarily, Searcy and Armijo[19] have pointed out how the freezing temperature of LiCl/KCl could be raised to 390 to 420°C in a polarised thermal battery, depending on the extent to which concentration gradients build up in it by the passage of different current levels. According to Newman[6], this same effect may lead to the predicted precipitation of the salt components within the electrodes of flooded cells.

Certainly, solidification can only occur at a higher temperature if the relative proportions of LiCl to KCl change without any contamination of the liquid by ions not already present in it. However the possibility also exists that ions such as sulphide or oxide, which are known to have some solubility in molten LiCl/KCl, may dissolve in it in heavily discharged batteries and have a depressant effect on solidification temperature.

Based on the apparent freezing point depression seen in earlier battery tests using internal thermocouples[4], all simulation curves shown in the Figures have been generated using 302-322°C as the notional freezing range of molten salt. However, since Table 1 shows that not all of the discharges were limited by temperature, it was expected (and confirmed by further model simulations using the theoretical freezing point of 352°C) that not all simulations would be affected by a change in assigned freezing point. Referring to Figs 7 and 8, the predicted discharges for Batteries 1 and 4 remained unaffected by an increase in freezing point from 302-322 to 352°C; that for Battery 2 improved even more after 400 s; that for Battery 6 was a definite improvement; whilst simulations for Batteries 3 and 5 were somewhat worsened.

The two discharges of Battery 11 seen in Fig 13 illustrate how the voltage-time model can be affected by assigned freezing temperature. When the simulations generated in Fig 13 using a freezing range of 322-302°C are compared with those of Fig 14 generated using the theoretical freezing point of 352°C, it is seen that the predicted discharge at the maximum ambient temperature remains unaffected by the change, indicating that the cell temperature in the model has not reached either freezing point. In contrast, an increase in assigned freezing point has improved the simulation of the discharge curve at the minimum ambient temperature, indicating that duration was predicted to be limited by cell temperature in this case. It is also noteworthy how well the model is able to predict the effect of ambient temperature on battery voltage earlier in the discharge, though after voltage 'spiking' has ended.

On balance, and in the absence of any allowance for the other heat sources mentioned in the next section, an assigned freezing point at or below the theoretical freezing point of 352°C (but not above it) seems best for obtaining the best prediction of battery duration in temperature-limited discharges. However, further study of this aspect would be desirable.

7.2 Other heat sources

Cooling rates of thermal batteries are designed to be small, so their cooling curves will automatically intersect any constant-temperature line at a glancing angle, so magnifying the uncertainty of when the voltage is predicted to collapse if the electrolyte freezing temperature is not precisely known. Another source of uncertainty arises if the slope of the cooling curve should be affected by extra heat sources. In deriving the simulations illustrated, the only heat sources taken into account were from the pyrotechnic burning, heating due to current flow inside the battery, and entropic cooling.

Rigorous theoretical treatments of heat sources within batteries have been given[20,21] which include a few effects not presently modelled. However, it was pointed out that some of these could be negligible for some types of battery. In any case, these treatments deal only with effects associated with the theoretical operation of the battery rather than with other unintended eventualities such as leakage currents or cathode pyrolysis. These latter may possibly dwarf some of the theoretical effects during thermal battery discharges.

Using curve-fitting procedures it was estimated that up to 58 cal of heat could be produced per gm of cell in a calcium/calcium chromate battery[2], representing about 30% of the heat output from the pyrotechnic. However, for a magnesium/iron disulphide battery, no extra heat had to be invoked to fit experimental data. Examples have been given[4] of lithium/iron disulphide batteries whose temperatures could also be modelled satisfactorily without recourse to extra heat generation.

Despite this, the rare occurrences of catastrophic failures of thermal batteries are a reminder that the energy of the electroactive materials is comparable with that of the pyrotechnic. A consideration of their thermodynamics, their electrical efficiency, and the rates of side reactions therefore helps to bracket the magnitude of any temperature-time effects. The Appendix indicates one way in which the scale of heat production from chemical side-reactions may be estimated. This first considers the total heat of chemical reaction if all the lithium metal were depleted; it then estimates, for the degradation rate of electrical capacity mentioned in section 6.1, how this scaled-down heat production rate might affect the cooling curves of the different batteries in Table 1. This analysis does not identify the mechanism of heat production, but linking it to the linear degradation rate discussed in section 6.1 would be consistent with either the continuous, slow direct chemical reaction recently postulated[12] between dissolved lithium and iron disulphide, or with slight but continuous shorting. It would not be so consistent with cathode pyrolysis which might be expected to peak early in the battery's active life.

The effects of this heat production rate were investigated for all of the batteries in Table 1. For the small Batteries 3, 5 and 6, it made an insignificant difference to the predicted cooling curve. The cooling rates of Batteries 1, 2 and 4 were slightly reduced, but those for Batteries 8 to 11 were significantly reduced as a result of chemical heat generation. The comparisons for three batteries are shown in Fig 15. The larger effects for Batteries 8 to 11 could be due to:

(i) the low surface/volume ratio for large cells, reducing heat loss;

(ii) the fact that very good insulation was used, because of the long duration requirements, which further reduced heat loss;

(iii) the fact that these lithium alloy batteries contained a higher weight percentage of lithium per cell, because of the desirability of discharging the battery on just one of the voltage plateaux of the alloy.

Of course, these calculations are for illustration only, and they might need to be modified if any of the assumptions made proved to be unwarranted. For example, not all of the lithium might be available to engage in exothermic reactions, or conversely other reducing agents like silicon, aluminium or powdered iron might also contribute to extra heat production.

It is seen from Fig 15 that the predicted time elapsed before some batteries (especially Battery 11) reached a fixed temperature would be longer where there was an extra heat source than without it. Also, when this effect is linked to freezing temperature (section 7.1) in order to predict the point at which voltage fall-off is expected, the freezing temperature in the model may need to be set higher when this heat source is incorporated than without it.

8 REMAINING DISCREPANCIES

Figs 6 to 14 show that the latest improvements made in the Mark III model have provided a net increase in the realism of the simulations for nearly all the batteries and test conditions which RAE possess information on. Even so, inspection of the Figures highlights the following features of the simulations requiring further improvement:

(i) the simulated durations may still be too optimistic for batteries which experience very high temperatures over a considerable time;

(ii) for batteries subjected to occasional pulses with open-circuit periods in between, the simulated voltage between each pulse does not fall away as it did in practice (Batteries 3 and 7, Fig 9). Also, the simulated voltage drops during the pulses do increase as the discharge proceeds, as observed, but the increases are too sudden and too large. Further study of the temperature-dependence of the electrical resistance of solidified electrolyte pellets might help to improve this;

(iii) whilst the treatment of time-dependent polarisation following application of a heavier load is adequate, the simulated magnitude of the

recovery curve after the load has been removed is too large (Battery 1).

9 CONCLUSIONS

(i) A further stage in the refinement of the RAE voltage-time model of thermal batteries has resulted in greater realism of the resulting simulations, over those produced by the previous version.

(ii) Application of the new model to a limited number but a wide range of battery types and test conditions has shown that both the overall voltage level and the internal resistance of the majority of batteries are estimated quite well, especially early in the discharge life, but diverge from the observed data later in life.

(iii) Pulse shapes may now be simulated better, though further improvement is necessary.

(iv) If the whole of the lithium in the anode (but no other reducing agent) is assumed to be available to engage in chemical side reactions, and the lithium is being depleted by this means at a rate of a fraction of a per cent per minute of active life, it is predicted that the heat release would scarcely reduce the cooling rates of many small to medium-sized batteries. However, it was predicted to very considerably reduce the cooling rate of some large, long-duration, well-insulated batteries containing lithium-alloy anodes. This might delay the point at which their voltages fell away due to freezing of molten salts.

(v) Whilst a reasonable simulation of performance over the whole range of battery types may be obtained by just one set of equations and parameter values, there are indications that further optimisation of the simulation for particular categories (such as the products of one particular manufacturer, or one particular combination of materials) may be possible by resetting parameter values individually for that category. Better simulations may then result when the model is applied to new battery applications within that category. A universal framework has been developed within which to do this - it would merely involve readjustment of numerical parameters based on discharge curves for a few typical batteries in each category.

(vi) The model is not intended to simulate the performance of those batteries which, through some manufacturing defect or other means, generate excessive heat or develop serious short-circuits. However, a steady continuous internal short may be simulated to predict its effect on both battery temperature and voltage.

Acknowledgments

The author would like to thank MSA (Britain) Ltd, Coatbridge, Scotland; SAFT (UK) Ltd, Hampton, England; and Sandia National Laboratories, Albuquerque, USA for permission to reproduce battery discharge curves as detailed in Table 1.

Appendix

ESTIMATED MAGNITUDE OF HEAT GENERATION FROM SIDE REACTIONS
(see section 7.2)

As a first approximation, it may be assumed that exotherms are generated by direct chemical reaction of lithium with either iron disulphide or with other materials such as oxides in the thermal insulation. Interaction with iron disulphide could either be by direct physical contact, or via pyrolysis generating sulphur vapour and migration of this to the anode. It could also occur by dissolution of the materials in electrolyte molten salts, and subsequent diffusion of these into the separator, as recently suggested[12]. Whatever the mechanism it is assumed that the heat release is the same as that calculated for the nominal discharge reaction, though brought about entirely by chemical means. This corresponds to the case where no useful electrical work is done, and where all the energy is wasted as internal heat.

The following treatment will assume an immobilised liquid-lithium anode in an electrically-balanced cell, according to the nominal chemical or electrochemical reaction

$$3Li + 2FeS_2 \rightarrow Li_3Fe_2S_4 \quad .$$

If the heat release from this may be approximated by the change in enthalpy at any temperature T, then literature values for the cell emf and its temperature coefficient may be used in the Gibbs-Helmholz equation to calculate the heat generation expected from complete conversion of the amounts shown by the above equation. This yields a value of 130 kcal, or ~6250 cal/gm of lithium metal.

For a cell containing about 2.25 wt% of lithium, the output would be ~140 cal/g of cell if all the lithium metal became exhausted by unproductive reaction. Assuming a weight-average cell specific heat of about 0.2 cal/g/^{o}C, and that all the active ingredients could be brought together instantly, the 'battery' would then approach a bomb calorimeter in behaviour, with an instant temperature rise of ~700^{o}C over and above that produced by the pyrotechnic. When a simulation was run for one of the batteries using the short-circuit option mentioned in section 5, and resistances of 1 MΩ and 1 mΩ were assigned for the external circuit and a continuous short down the battery central axis respectively, the temperature was predicted to rise by about 660^{o}C after 1 min. This is in line with the temperature rise calculated above.

With regard to the observed slow degradation of capacity mentioned in section 6.1, this same heat output may be scaled down in the model (a) to that fraction of the battery's capacity which is degrading, and (b) spread out over the

Table 1

DETAILS OF BATTERIES AND TEST CONDITIONS

Battery number	Manufacturer	Figure ref.	Anode type	Outside diameter (mm)	Load type	Predicted factor limiting life
1	MSA (Britain)	1,5,7,15	Li	89	a*	Capacity
2	SAFT (UK)	2,6,8,15	LiAl	62	b	Marginal
3	MSA (Britain)	2,6,8 3,9	Li	42	c a*	Temperature Temperature
4	SAFT (UK)	2,6,8	LiAl	32	b	Marginal
5	SAFT (UK)	2,6,8	LiAl	32	b	Temperature
6	MSA (Britain)	2,6,8	Li	18	c**	Temperature
7	MSA (Britain)	3,9	Li	50	a	Temperature
8	Sandia Labs	10,11	LiSi	73	c	Capacity
9	Sandia Labs	12	LiSi	76	c	Temperature
10	Sandia Labs	12	LiSi	51	c	Temperature
11	Sandia Labs	13,14,15	LiSi	91	c	Capacity (70°C) Temp (-35°C)

Key: a, constant currents with intermittent pulses

b, continuous constant current(s)

c, continuous constant resistive load(s)

*, tested by RAE; the test on Battery 3 used a special thermal insulating jacket around the battery to minimise heat loss

**, the figures show discharges at both ambient temperature extremes

Li, this represents unalloyed immobilised liquid lithium

Literature references to Sandia Laboratories batteries:

Battery 8: Fig 8 of Ref 18
Battery 9: Battery 228 in Fig 5 of Ref 19
Battery 10: Fig 31a of Ref 15
Battery 11: Fig 4 of Ref 22

REFERENCES

No.	Author	Title, etc
1	A. Attewell A.J. Clark	A review of recent developments in thermal batteries. Power Sources 8 (Academic Press, J Thompson, Ed), International Power Sources Symposium Committee, pp 285-303 (1981)
2	D.M. Bush R.L. Hughes	A thermal model of a thermal battery. Sandia Laboratories Technical Report SAND 79-0834 July 1979
3	J. Knight I. McKirdy	The prediction and measuremant of thermal battery internal temperatures during and after activation. Power Sources 11 (L.J. Pearce, Ed.), International Power Sources Symposium Committee, pp 491-507 (1987)
4	J. Knight I. McKirdy	The validation of a thermal battery model using electrically-inert and -active batteries. Proceedings of the 34th International Power Sources Symposium, 25-28 June 1990 (US Army Laboratory Command and IEEE, Sponsors), pp 141-144
5	J.P. Pemsler R.K.F. Lam J.K. Litchfield S. Dallek B.F. Larrick B.C. Beard	Discharge behaviour and thermal stability of synthetic FeS_2 cathode material. *J. Electrochem. Soc.*, 137, (1), pp 1-7 (1990) (and references therein)
6	D. Bernardi J. Newman	Mathematical modelling of lithium (alloy), iron disulphide cells. *J. Electrochem. Soc.*, 134, 6, pp 1309-1318 (1987)
7	R. Pollard J. Newman	Mathematical modelling of the lithium-aluminium iron sulphide battery, Parts I and II. *J. Electrochem. Soc.*, 128, 3, pp 493-507 (1981)
8	C.M. Shepherd	Design of primary and secondary cells. II. An equation describing battery discharge. *J. Electrochem. Soc.*, 112, (7), pp 657-664 (1965)
9	L. Redey J.A. Smaga J.E. Battles R. Guidotti	Investigation of primary Li-Si/FeS_2 cells. Argonne National Laboratory Report ANL-87-6, April 1987 (U)

REFERENCES (continued)

No.	Author	Title, etc
10	C.J. Wen B.A. Boukamp R.A. Huggins W. Weppner	Thermodynamic and mass transport properties of 'LiAl'. *J. Electrochem. Soc.*, 126, (12), pp 2258-2266 (1979)
11	J. Knight	Unpublished RAE studies.
12	R.A. Guidotti F.W. Reinhardt J.A. Smaga	Self-discharge study of Li-alloy/FeS_2 thermal cells. Proc. 34th International Power Sources Symposium, 25-28 June 1990, (US Army Laboratory Command and IEEE, Sponsors), pp 132-135
13	A.C. Conry	Private communication
14	S.P.S. Badwall R.J. Thorn	Conductivities and electronic structures of some phases in the lithium-iron-sulphur system. *J. Solid State Chem.*, 43, p 163 (1982)
15	R.A. Guidotti F.W. Reinhardt W.F. Hammetter	Screening study of lithiated catholyte mixes for a long-life Li(Si)/FeS_2 thermal battery. Sandia Laboratories Report SAND85-1737, December 1988 (U)
16	A.G. Ritchie	Unpublished RAE results
17	L. Redey M. McParland R. Guidotti	Resistivity measurements of halide-salt/MgO separators for thermal cells. Proceedings of the 34th International Power Sources Symposium, 25-28 June 1990 (US Army Laboratory Command and IEEE, Sponsors), pp 128-131
18	R.K. Quinn A.R. Baldwin J.R. Armijo P.G. Neiswander D.E. Zurawski	Development of a lithium alloy/iron disulphide, 60-minute primary thermal battery. Sandia Laboratories Technical Report SAND79-0814, April 1979 (U)
19	J.Q. Searcy J.R. Armijo	Improvements in Li(Si)/FeS_2 thermal battery technology. Sandia Laboratories Technical Report SAND82-0565, June 1982 (U)
20	D. Bernardi E. Pawlikowski J. Newman	A general energy balance for battery systems. *J. Electrochem. Soc.*, 132, 1, pp 5-12 (1985)

REFERENCES (concluded)

No.	Author	Title, etc
21	H.F. Gibbard	Thermal properties of battery systems. *J. Electrochem. Soc.*, 125, 3, pp 353-358 (1978)
22	H.K. Street	Characteristics and development report for the MC3573 thermal battery. Sandia Laboratories Technical Report SAND82-0695, February 1983 (U)

Fig 1

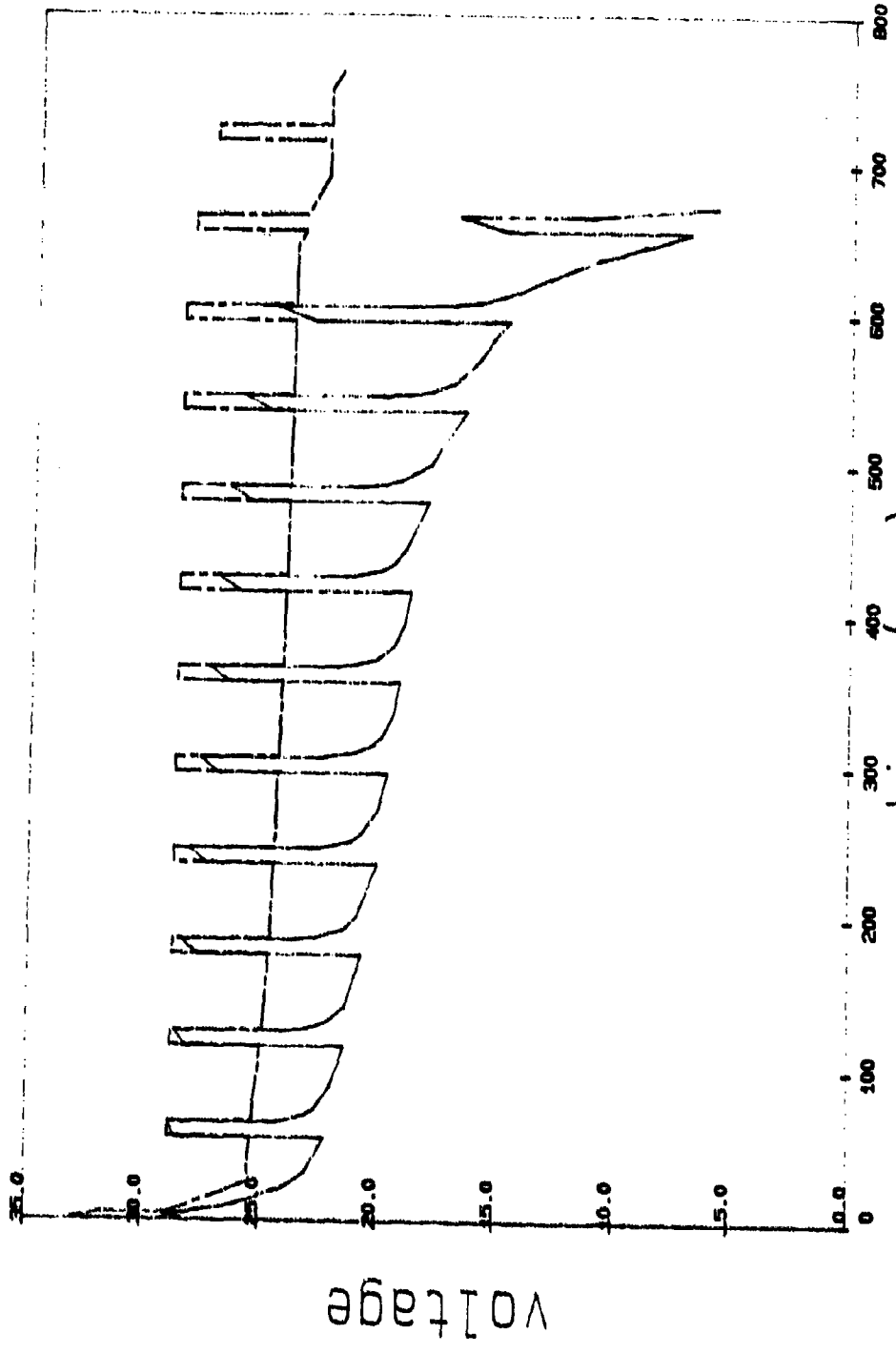

Fig 1 Application of Mark II model to a heavy pulsed discharge of Battery 1

TM Mat/Btr 1163

Fig 2

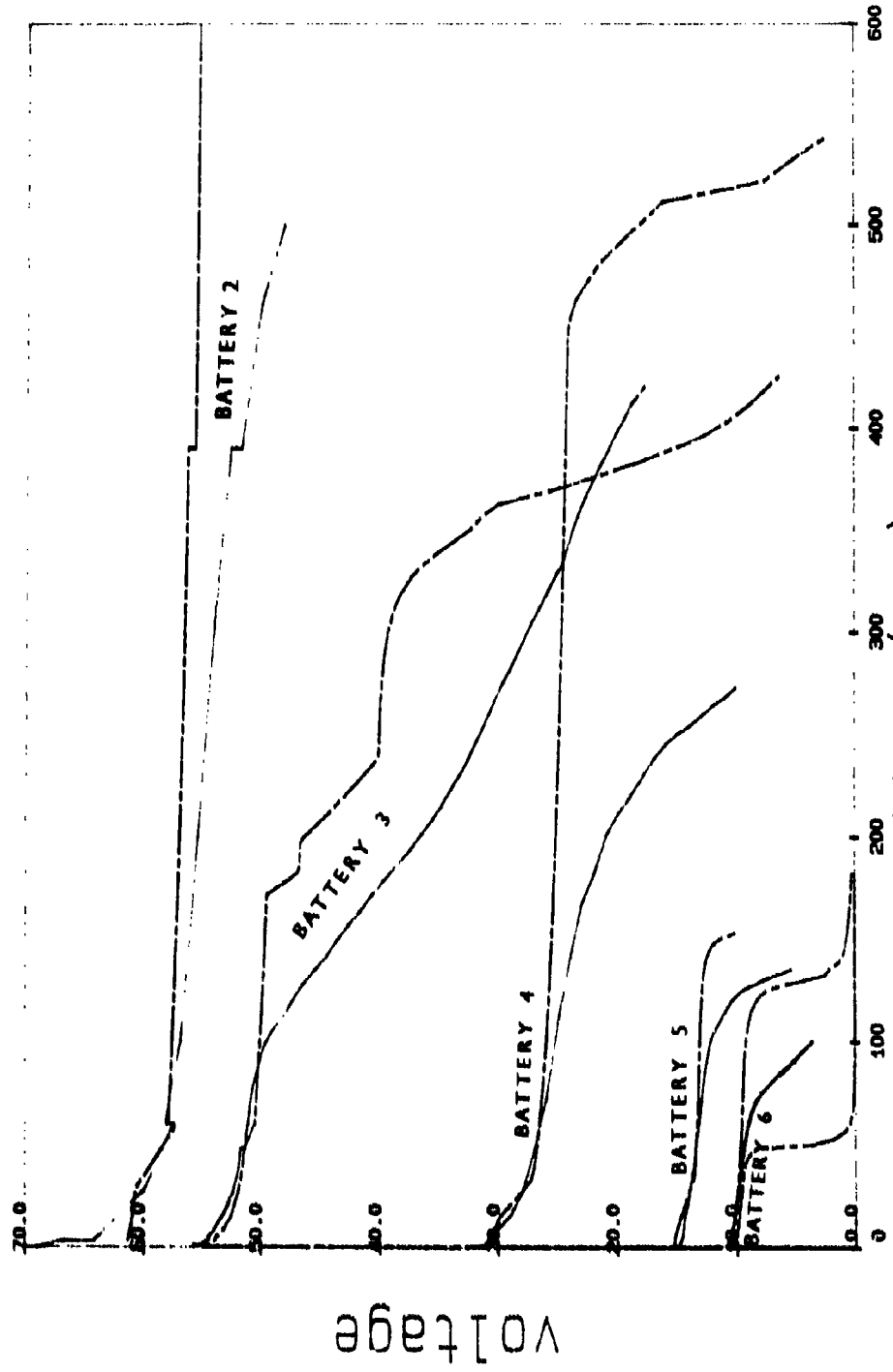

Fig 2 Application of Mark II model to some discharges of Batteries 2-6

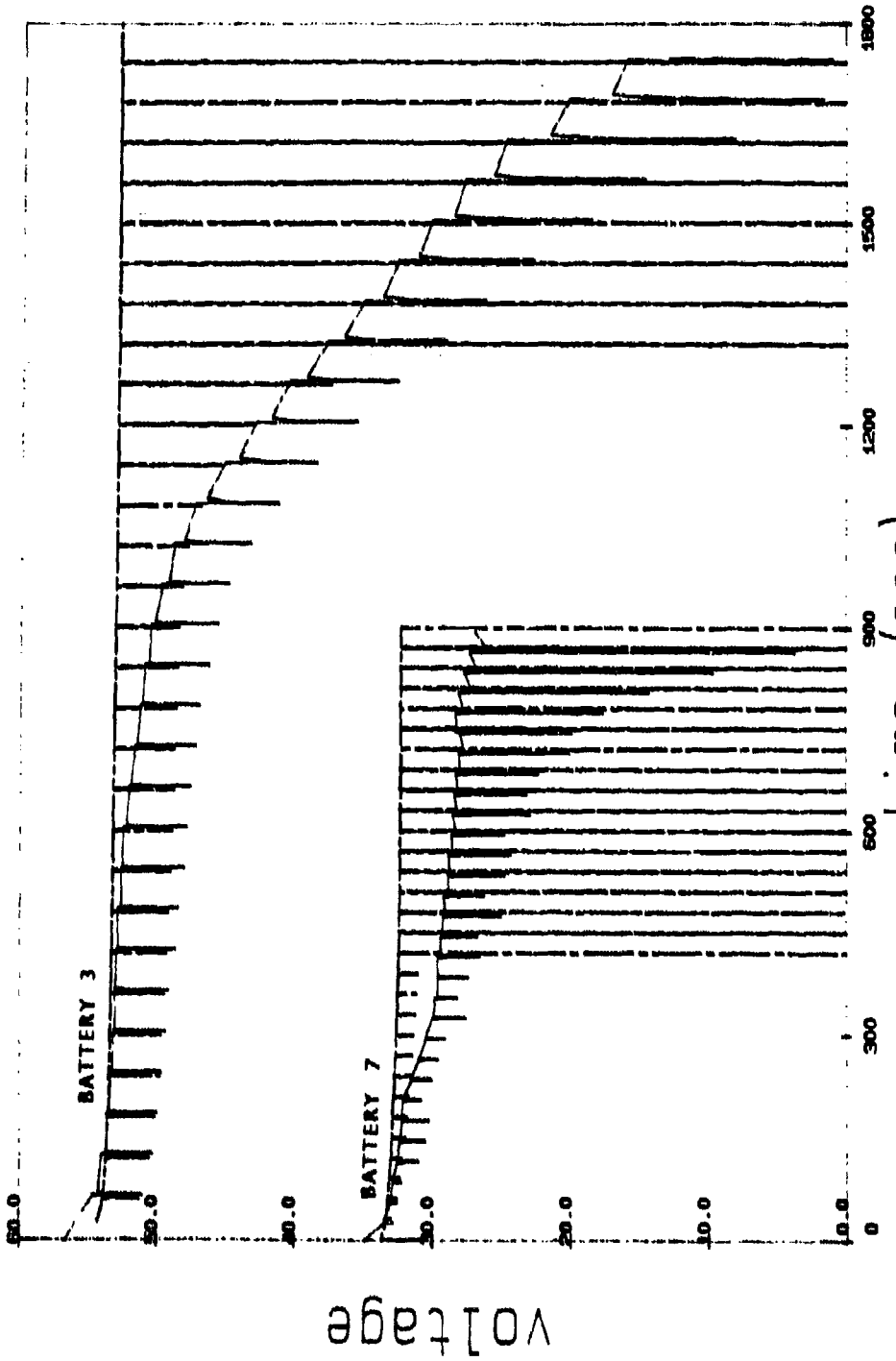

Fig 3 Application of Mark II model to pulsed discharges of Batteries 3 and 7

Fig 4

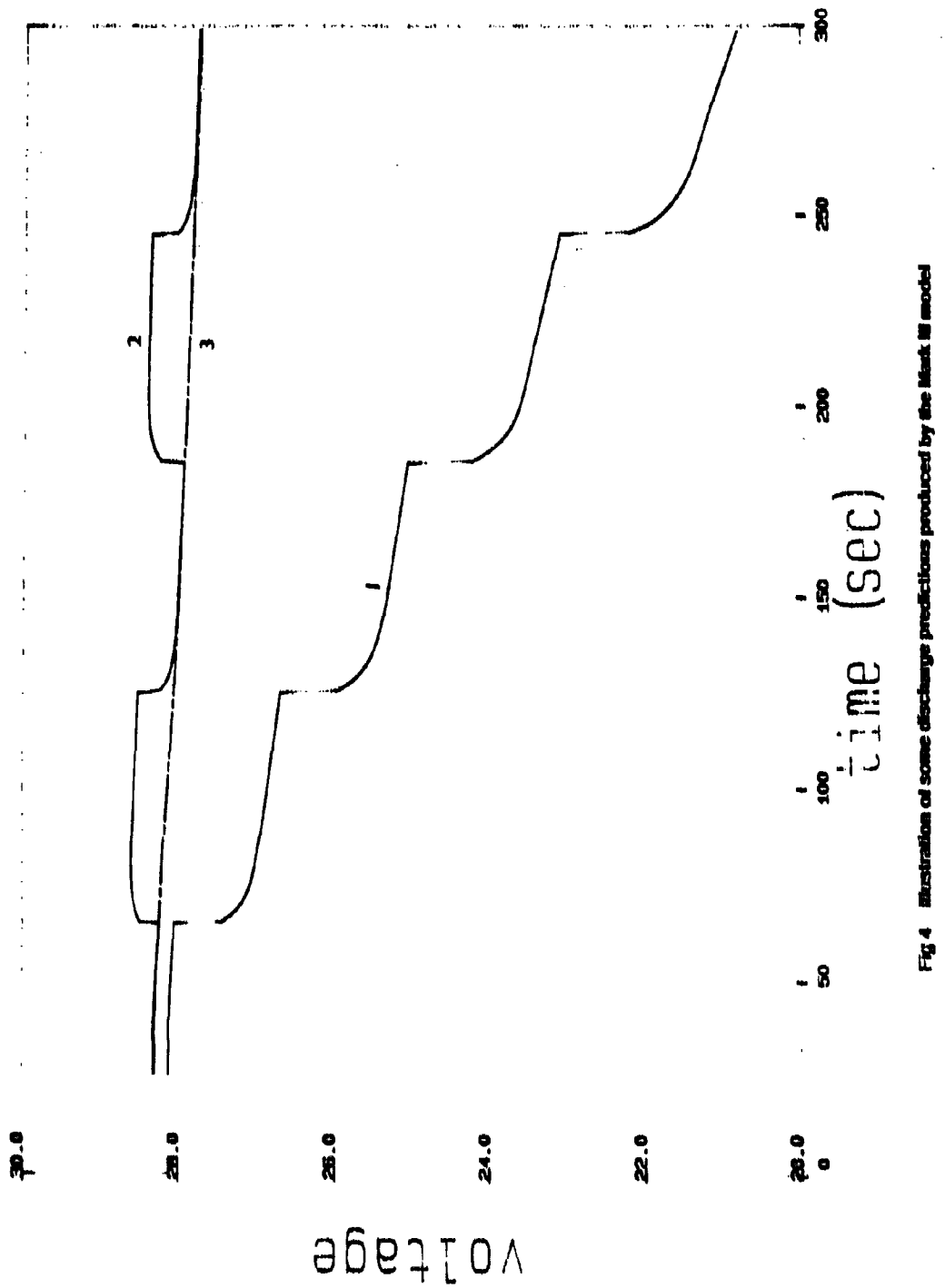

Fig 4 Illustration of some discharge predictions produced by the Mark III model

Fig 5

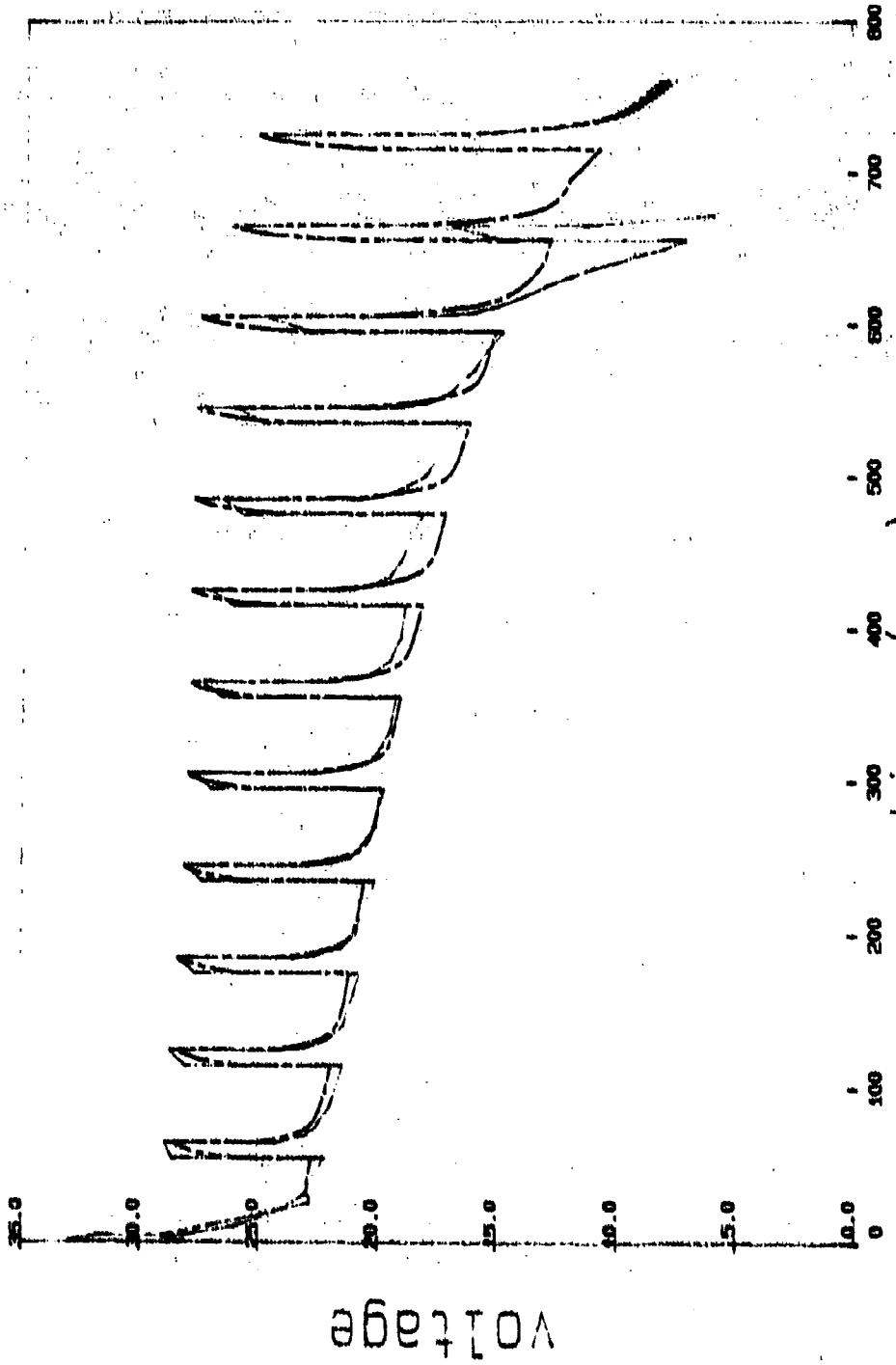

Fig 5 Application of Mark III model using equation 3 to pulse discharge of Battery 1

Fig 6

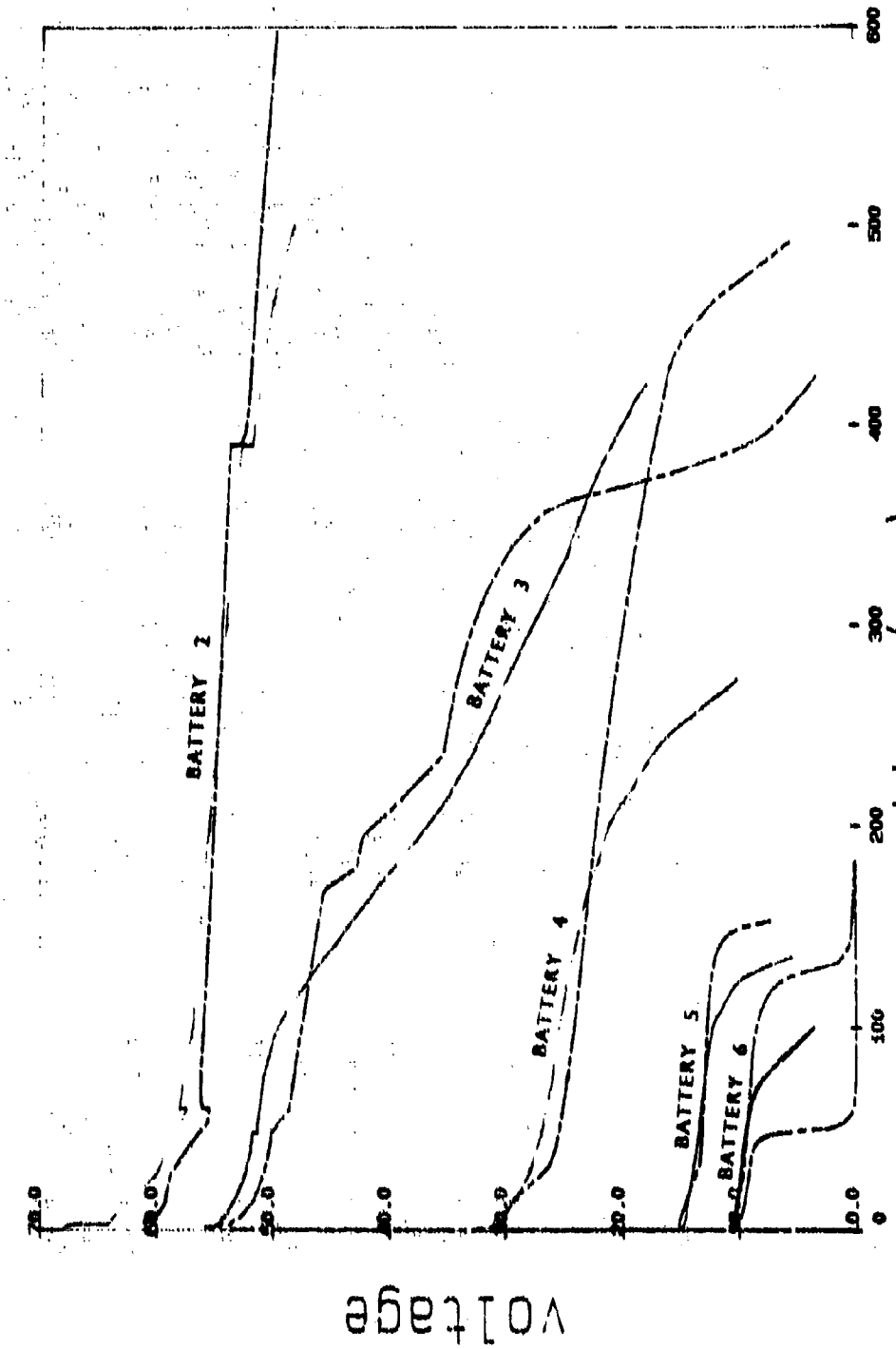

Fig 6 Application of Mark II model using equation 3 to Batteries 2-6

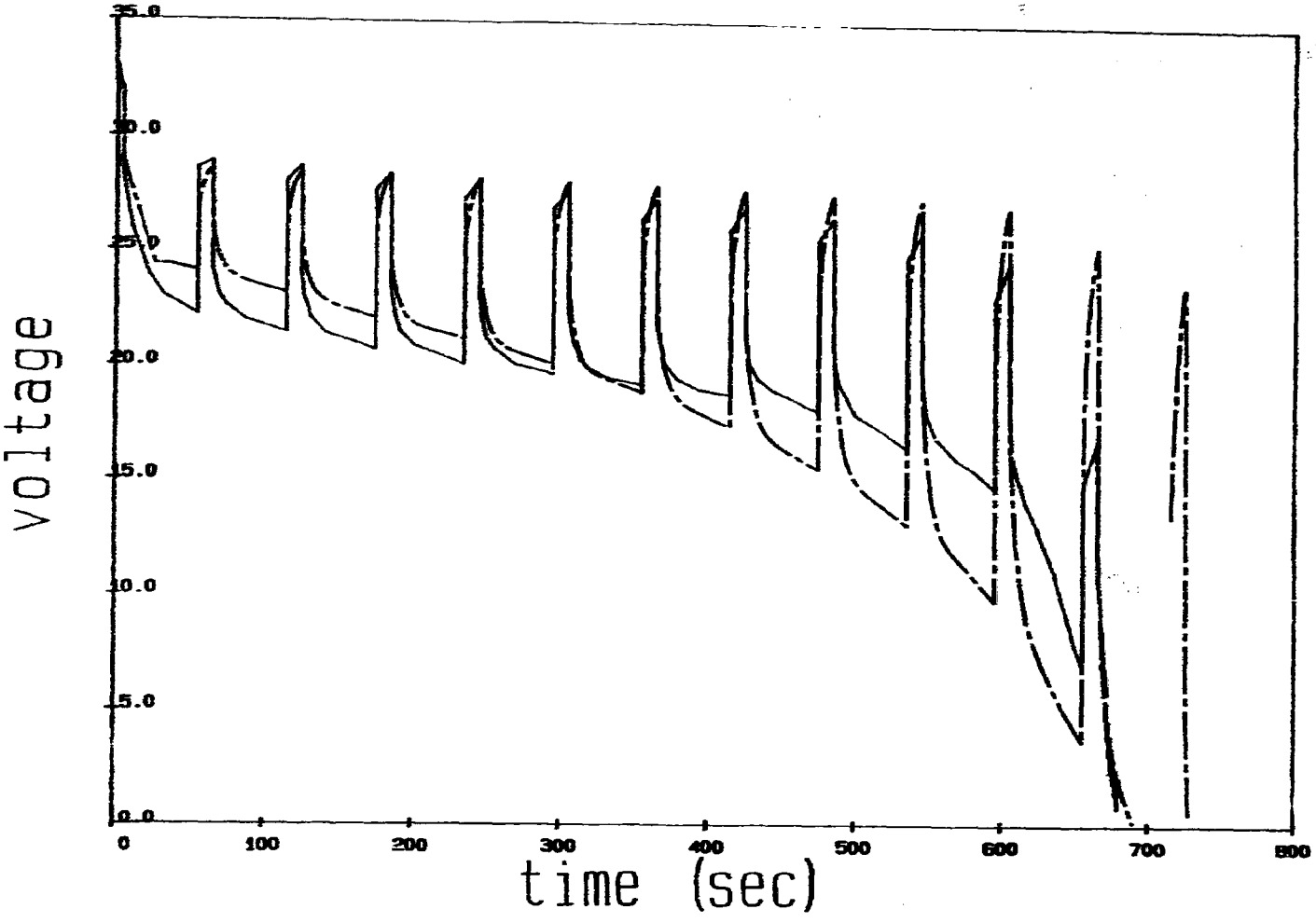

Fig 7 Application of Mark III model using equation 5 to pulse discharge of Battery 1

Fig 8

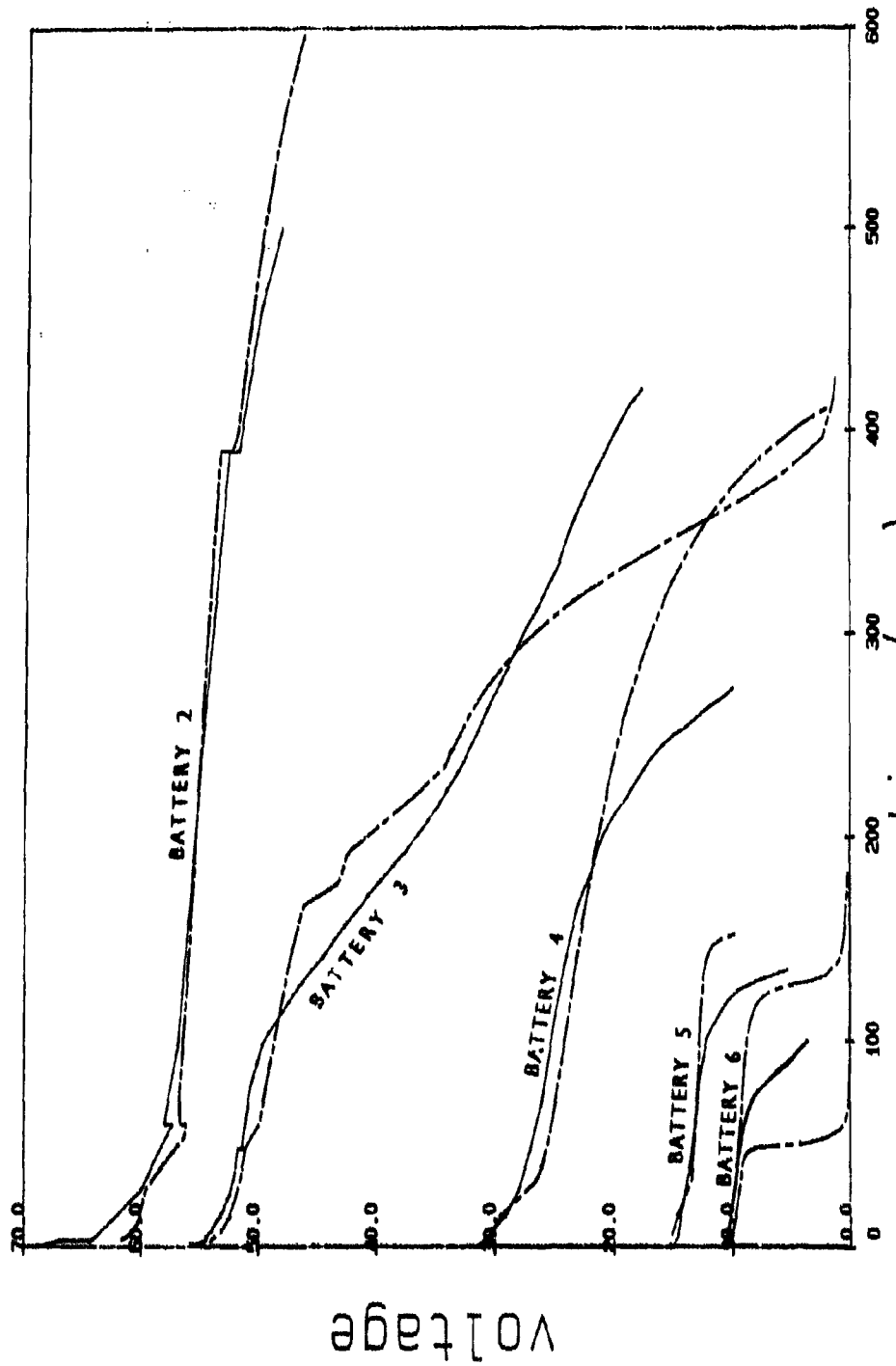

Fig 8 Application of Mark III model using equation 5 to Batteries 2-6

Fig 9

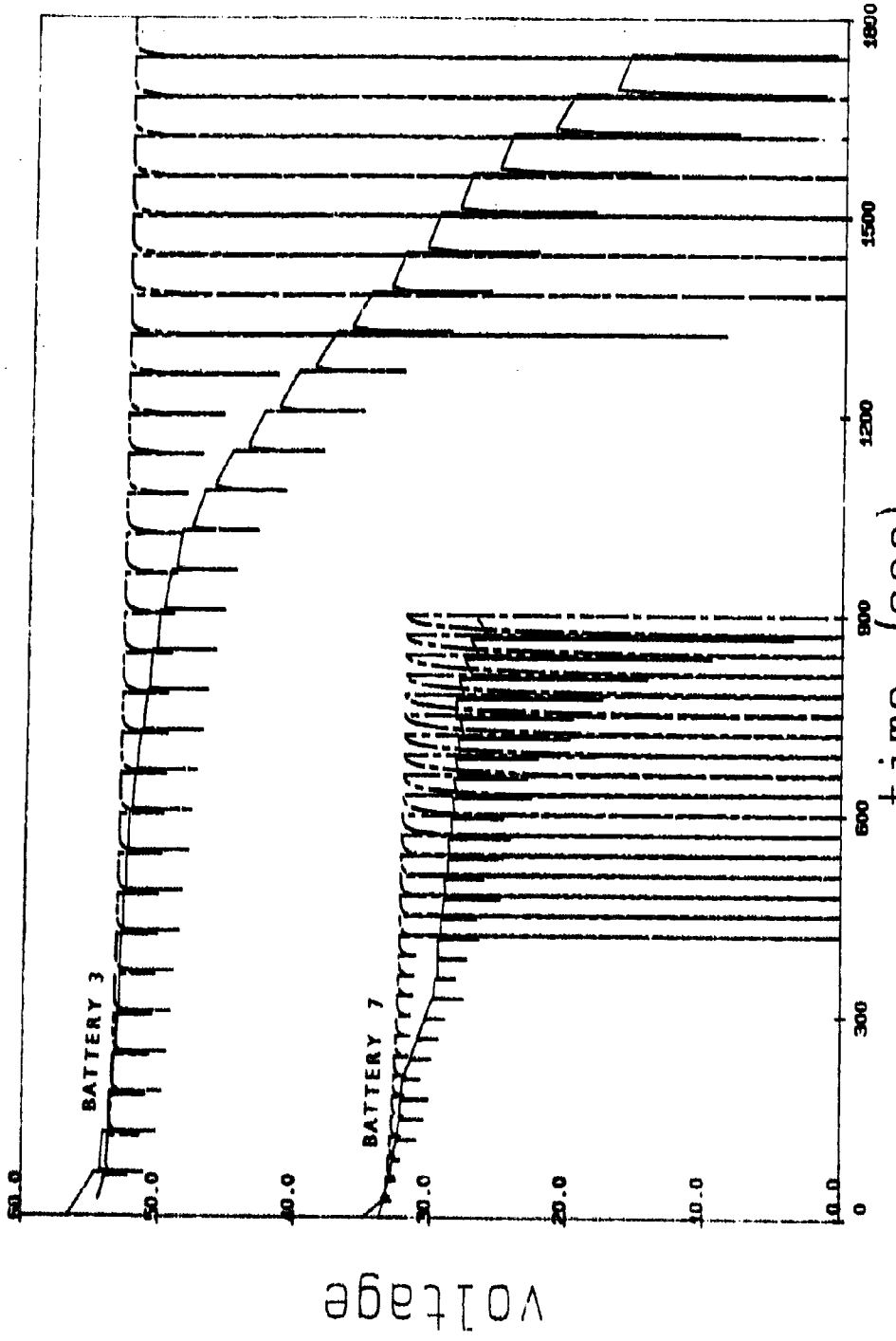

Fig 9 Application of Mark III model using equation 5 to pulsed discharges of Battery 3 and 7

TM Mat/Btr 1163

Fig 10

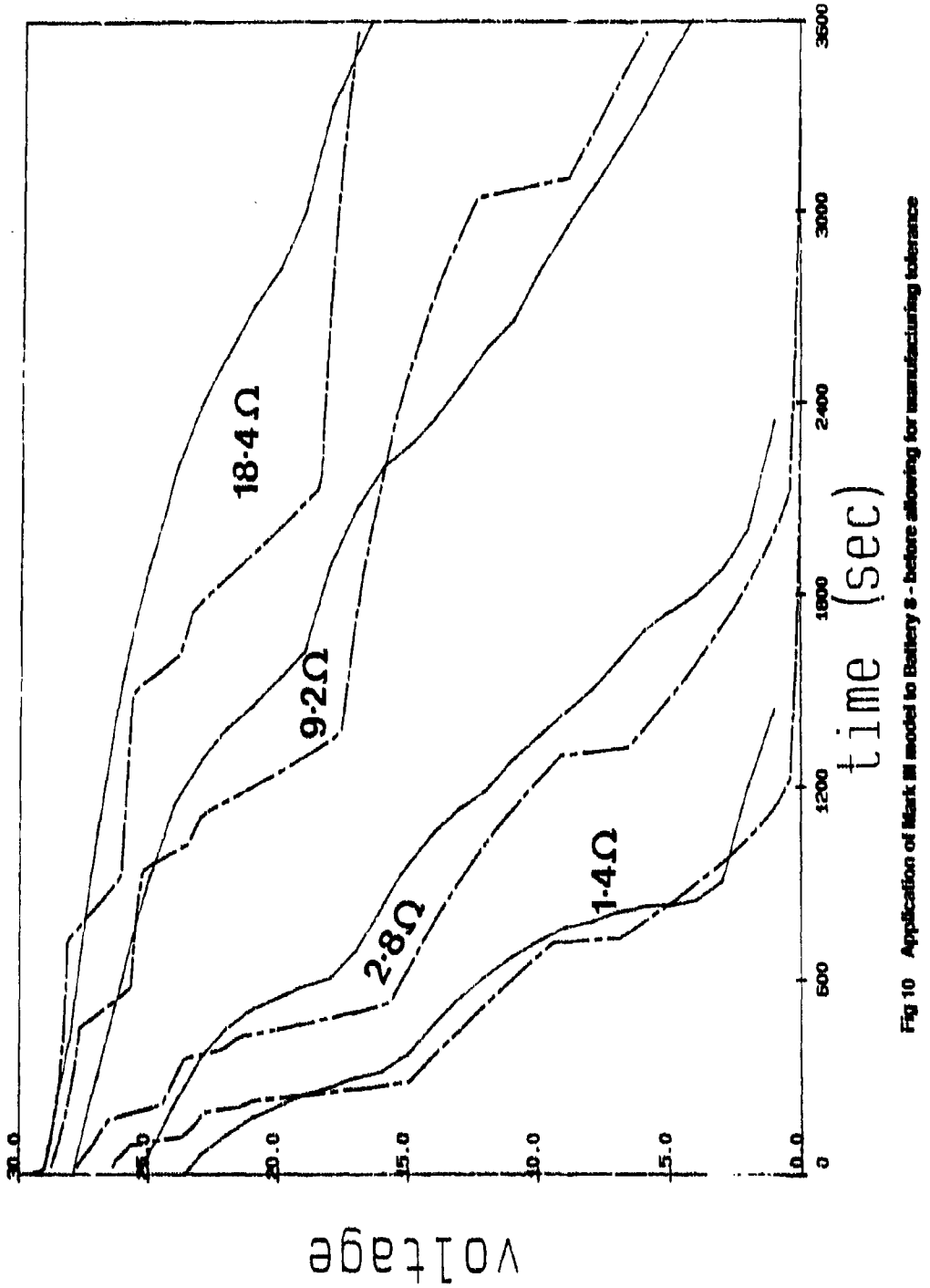

Fig 10 Application of Mark III model to Battery 8 - before allowing for manufacturing tolerance

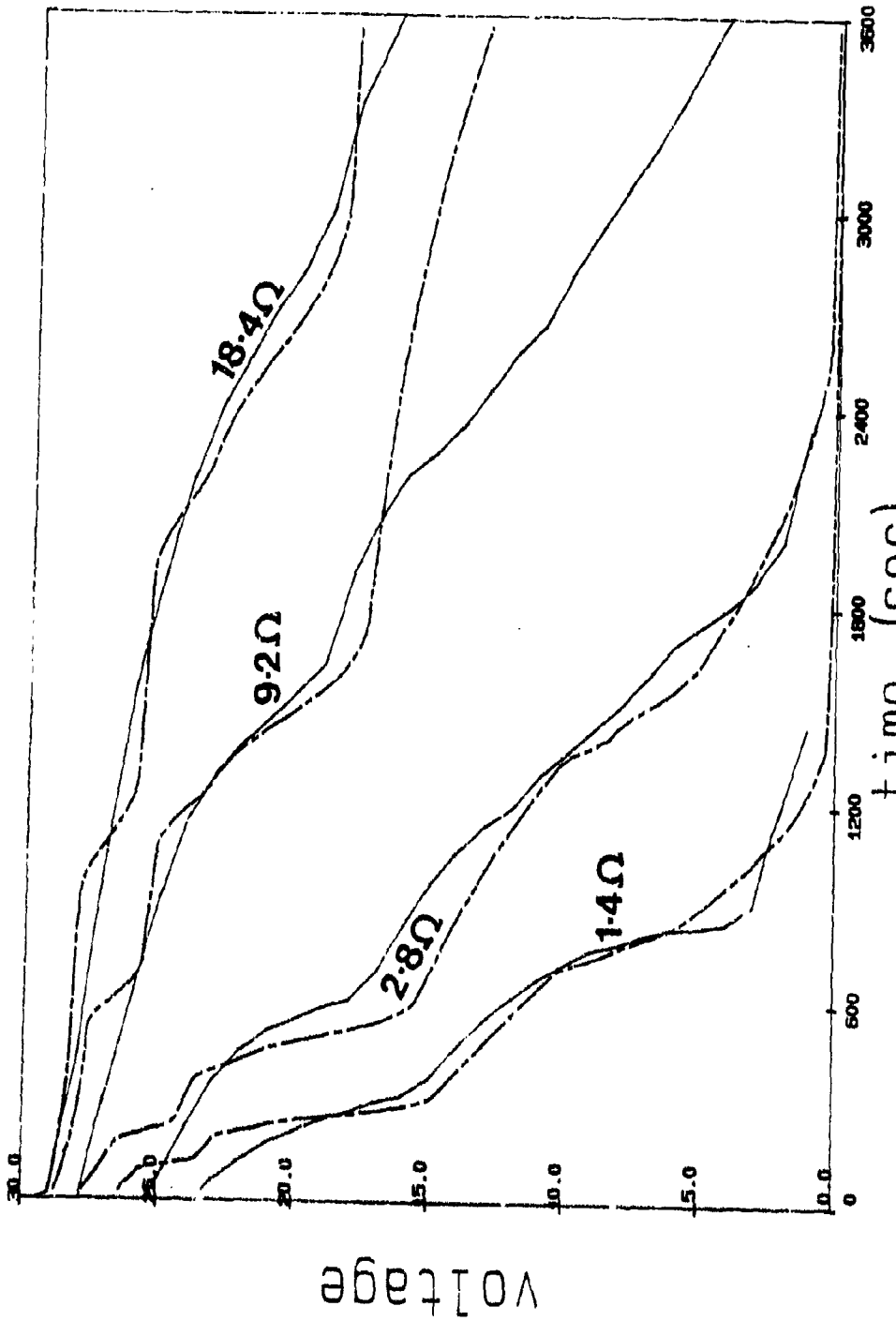

Fig 11 Effect of manufacturing tolerance (and lower degradation rate) on predictions for Battery 8

Fig 12

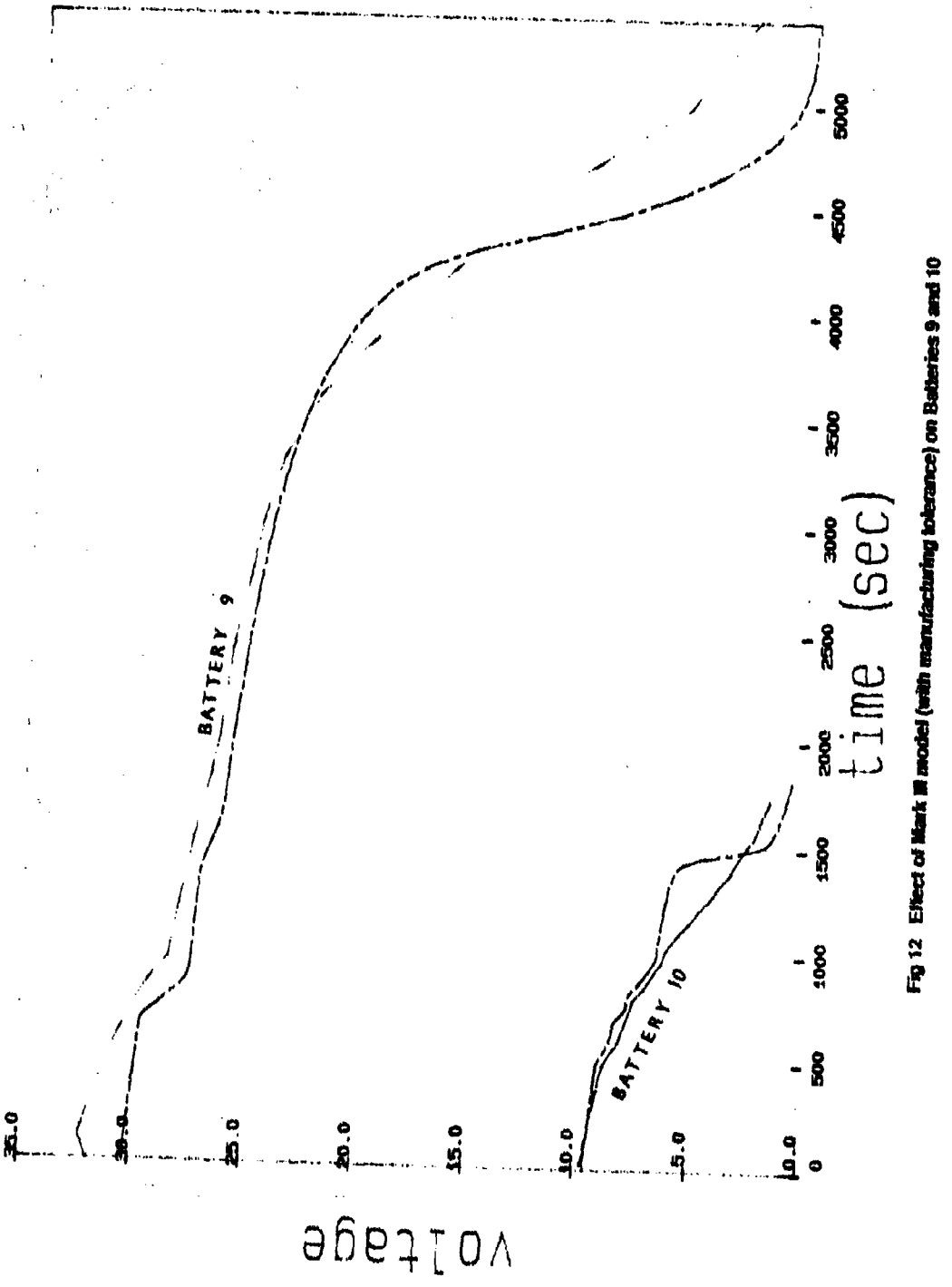

Fig 12 Effect of Mark III model (with manufacturing tolerance) on Batteries 9 and 10

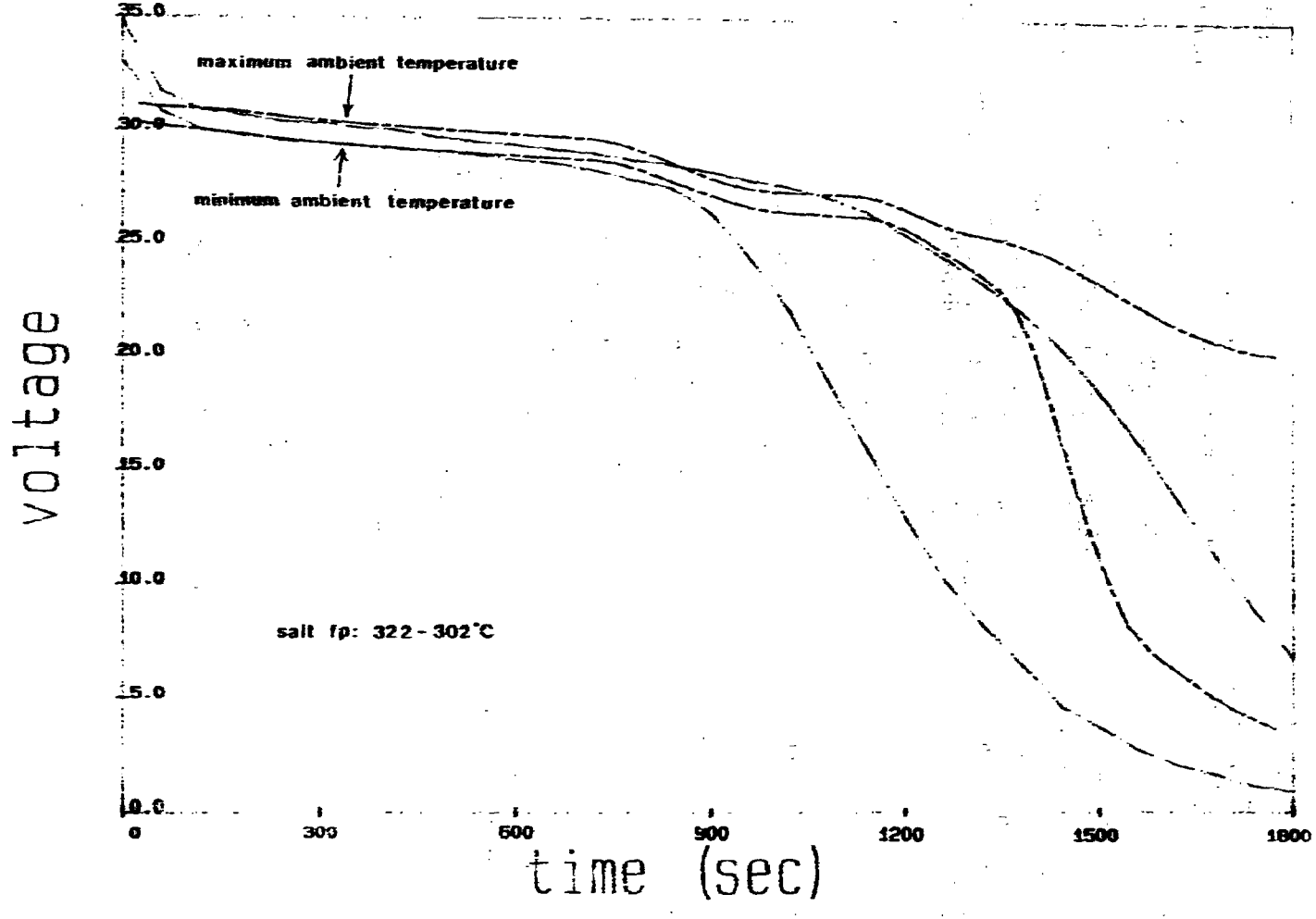

Fig 13 Predictions for Battery 11 at two different ambient temperatures

Fig 13

Fig 14

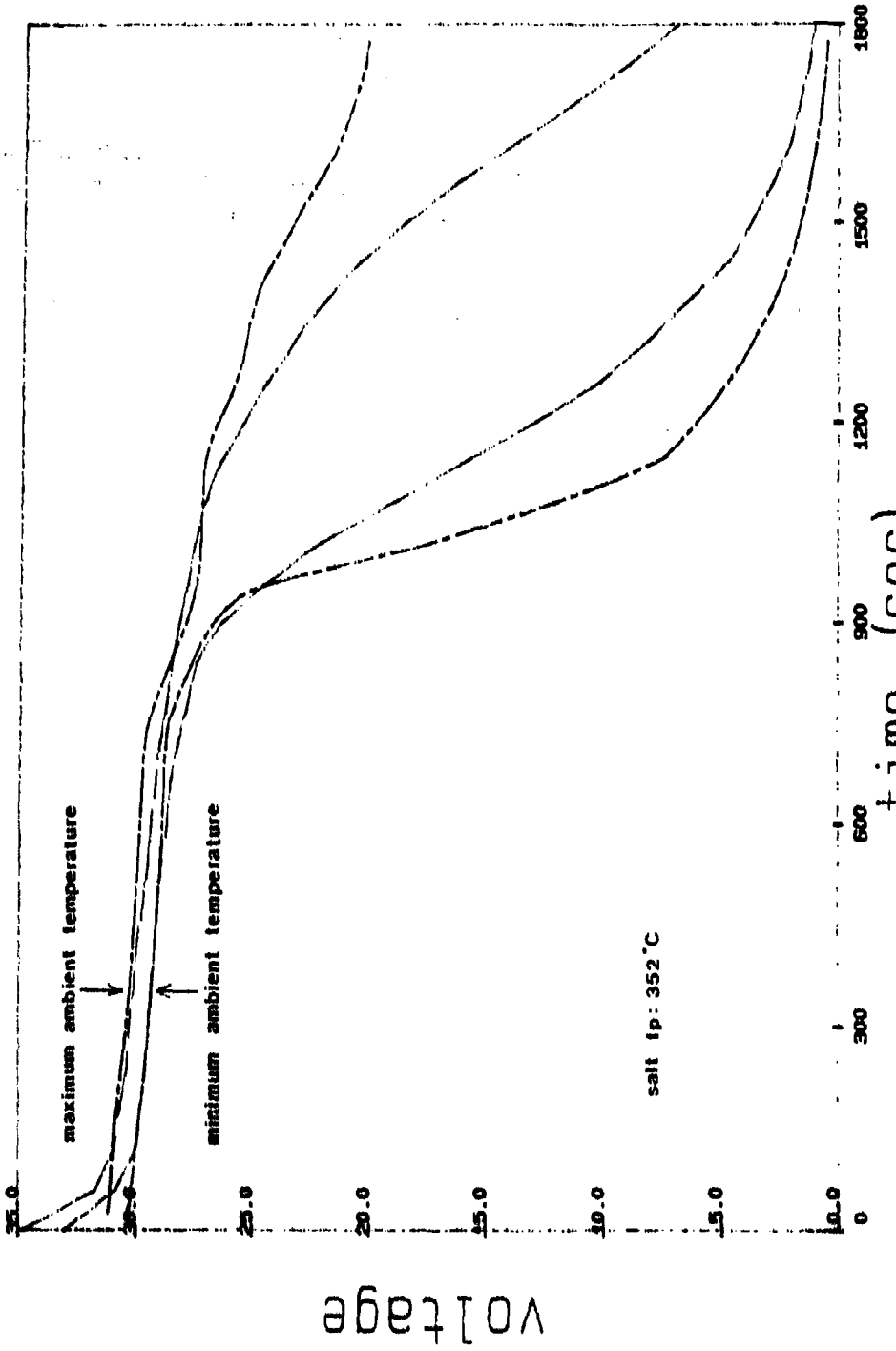

Fig 14 Effect of changed salt freezing point on predictions for Battery 1f

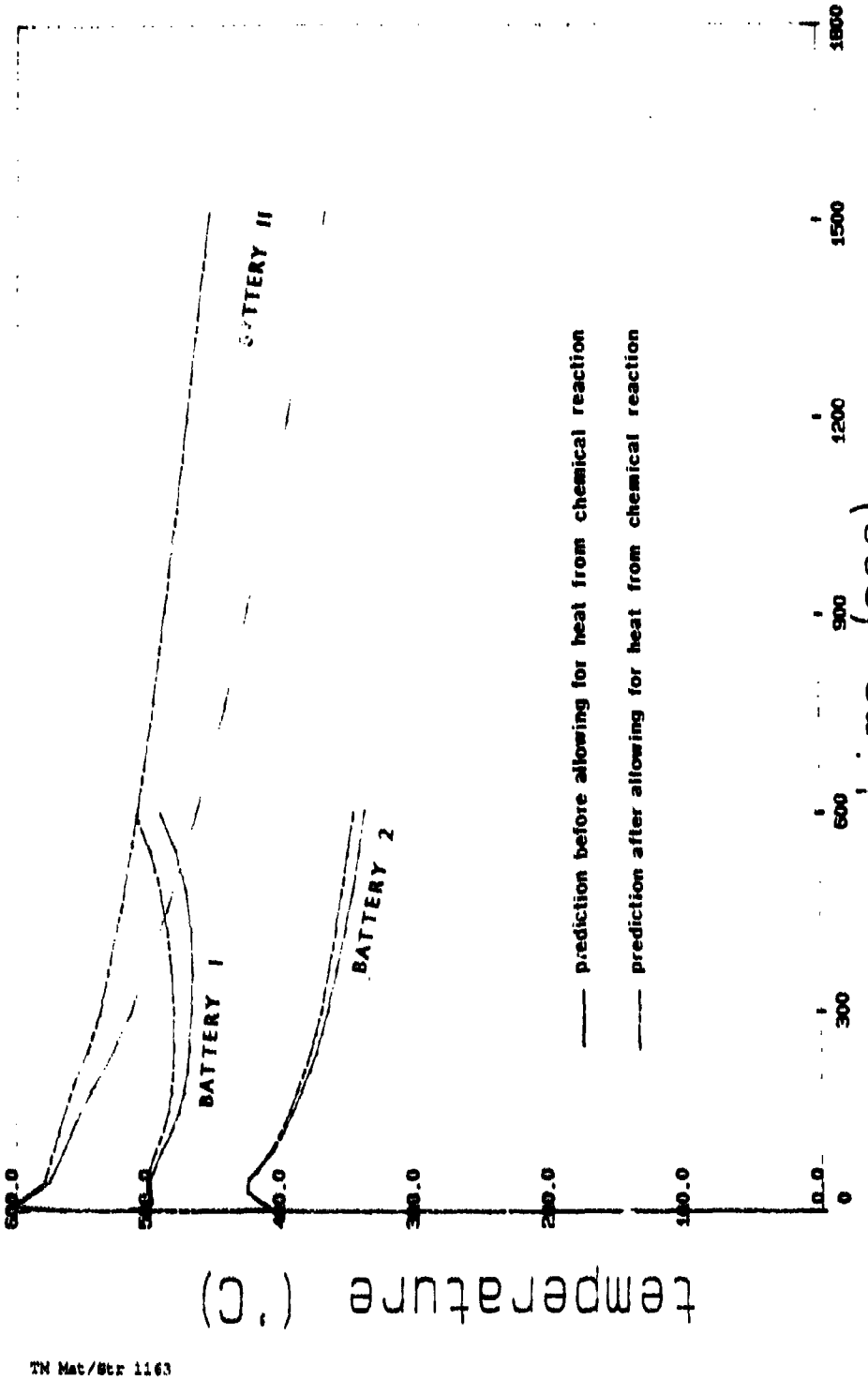

Fig 15 Effect of chemical side reactions on predicted cooling curves for three batteries

REPORT DOCUMENTATION PAGE

Overall security classification of this page

UNLIMITED

As far as possible this page should contain only unclassified information. If it is necessary to enter classified information, the box above must be marked to indicate the classification, e.g. Restricted, Confidential or Secret.

1. DRIC Reference (to be added by DRIC)	2. Originator's Reference	3. Agency Reference	4. Report Security Classification/Marking
	RAE TM Mat/Str 1163		UNLIMITED

5. DRIC Code for Originator	6. Originator (Corporate Author) Name and Location
7673000W	Royal Aerospace Establishment, Farnborough, Hants, UK
5a. Sponsoring Agency's Code	6a. Sponsoring Agency (Contract Authority) Name and Location

7. Title
Evolution of a voltage-time model of thermal batteries

7a. (For Translations) Title in Foreign Language

7b. (For Conference Papers) Title, Place and Date of Conference

8. Author 1. Surname, Initials	9a. Author 2	9b. Authors 3, 4	10. Date	Pages	Refs.
Knight, J.			February 1991	44	22

11. Contract Number	12. Period	13. Project	14. Other Reference Nos.

15. Distribution statement
(a) Controlled by --

(b) Special limitations (if any) --

If it is intended that a copy of this document shall be released overseas refer to RAE Leaflet No.3 to Supplement 6 of MOD Manual 4.

16. Descriptors (Keywords) (Descriptors marked * are selected from TEST)

Thermal batteries. Modelling.

17. Abstract

A temperature-time model of thermal batteries has almost been completed and validated against experimental data. This Memorandum first summarises early attempts to integrate a voltage-time model into this, taking advantage of the instantaneous predictions of temperature, thermodynamic potentials, and internal resistance which the thermal model provides. It then describes how recent refinements of the voltage-time model have led to improved simulation of the discharges of a wide range of sizes and types of thermal battery under an equally wide range of test conditions.

The semi-empirical approach adopted has been to provide a universally-applicable framework based on logical concepts to cover various effects such as polarisation etc, but with adjustable numerical parameters. It is shown that a moderately good simulation may be obtained for the majority of available discharge curves, using this one set of equations and without altering parameter values. Further improvements can be obtained when parameter values are optimised for one particular type of battery.

F5910/1